



# **ECG classification based on wavelet analysis**

**by Emmanouil Sifakis**

December 2003

Department of Electronics Engineering & Computer Engineering  
Technical University of Crete

## ABSTRACT

A classification algorithm based on wavelet transform analysis has been developed in order to detect ECG characteristics concerning some of the most common types of arrhythmias encountered in the majority of the human population. In particular, sinus tachycardia, sinus bradycardia, premature contractions, atrial fibrillation (AF) and the malignant ventricular tachyarrhythmias (VT) may be discriminated by this single uniform classification algorithm. The results showed that the proposed method is a promising approach as it had correctly detected 98.4% of the VT and 82.5% of the AF recordings, while the overall success rate was 91%.

## ACKNOWLEDGEMENTS

I am grateful to Dr. Michalis Zervakis for his help and encouragement during the course of this project. His expertise and guidance have been invaluable.

I would also like to thank Dr. Konstantinos Kalaitzakis for overseeing this project work and allowing me to act independently.

I would also like to give my thanks to cardiologist Dr. George Makrakis for his help. His advice has been precious to the successful completion of the project.

I am also grateful to my brother and my parents for their support.

# TABLE OF CONTENTS

	<b>Page</b>	
<b>CHAPTER 1</b>	<b>MEDICAL BACKGROUND</b>	<b>5</b>
<b>1.1</b>	<b>The heart</b>	<b>5</b>
1.1.1	Basic structure	5
1.1.2	The conduction system	5
<b>1.2</b>	<b>The electrocardiogram (ECG)</b>	<b>6</b>
1.2.1	The 12-lead ECG	6
1.2.2	ECG individual components	8
1.2.3	Heart rate	9
1.2.4	Heart rhythm	10
<b>1.3</b>	<b>Arrhythmias</b>	<b>11</b>
1.3.1	Introduction	11
1.3.2	Sinus tachycardia (ST)	11
1.3.3	Sinus bradycardia (SB)	12
1.3.4	Premature contractions (PC)	13
1.3.4.1	Premature atrial contractions (PAC)	13
1.3.4.2	Premature ventricular contractions (PVC)	14
1.3.5	Atrial fibrillation (AF)	14
1.3.6	Ventricular tachyarrhythmia (VT)	15
1.3.6.1	Monomorphic ventricular tachycardia	16
1.3.6.2	Polymorphic ventricular tachycardia: Ventricular fibrillation (VF)	16
<b>CHAPTER 2</b>	<b>ALGORITHMS OVERVIEW</b>	<b>18</b>
<b>2.1</b>	<b>Fourier transform</b>	<b>18</b>
2.1.1	Continuous-time Fourier transform (CFT)	18
2.1.2	Short-time Fourier transform (STFT)	19
<b>2.2</b>	<b>Wavelet transform</b>	<b>21</b>
2.2.1	Wavelets overview	21
2.2.2	Wavelet theory	23
2.2.3	Continuous wavelet transform (CWT)	25
2.2.4	CWT versus STFT	28

2.2.5	Discrete wavelet transform (DWT)	28
2.2.6	CWT versus DWT	31
<b>CHAPTER 3</b>	<b>IMPLEMENTATION</b>	<b>33</b>
<b>3.1</b>	<b>Data acquisition</b>	<b>33</b>
<b>3.2</b>	<b>Data analysis</b>	<b>34</b>
3.2.1	Pre-processing	34
3.2.2	Wavelet transform (WT)	35
3.2.3	Post-processing	38
3.2.3.1	Wavelet power spectrum (WPS)	38
3.2.3.2	Global power spectrum (GPS)	39
3.2.3.3	Scale-averaged wavelet power spectrum (SAWPS)	40
3.2.3.4	GWS analysis	41
3.2.3.5	VT detection	43
3.2.3.6	AF detection	46
3.2.3.7	PC detection	49
3.2.3.8	HR estimation	50
3.2.3.9	ST, SB and NSR detection	50
3.2.4	Classification	51
<b>3.3</b>	<b>Software presentation</b>	<b>52</b>
3.3.1	Input variables	52
3.3.2	Program output	54
<b>CHAPTER 4</b>	<b>RESULTS</b>	<b>57</b>
<b>4.1</b>	<b>Parameters distribution</b>	<b>57</b>
4.1.1	Distribution of the VT parameters	57
4.1.2	Distribution of the AF parameters	62
<b>4.2</b>	<b>ECG classification results</b>	<b>66</b>
<b>4.3</b>	<b>ECG classification rates</b>	<b>67</b>
<b>CHAPTER 5</b>	<b>CONCLUSION AND FURTHER WORK</b>	<b>71</b>
<b>CHAPTER 6</b>	<b>REFERENCES</b>	<b>73</b>
<b>CHAPTER 7</b>	<b>APPENDIX</b>	<b>76</b>

## 1. MEDICAL BACKGROUND

### *1.1 The heart*

#### *1.1.1 Basic structure*

The human heart is a muscular organ, which is located just to the left of the breast bone. There are four chambers inside the heart that fill with blood. Two of these cavities are called atria and the other two are called ventricles. The two atria that receive blood from the body or lungs form the curved top of the heart. The ventricles meet at the bottom of the heart to form a pointed base. The right ventricle pumps blood to the lungs to pick up oxygen whereas the left ventricle pumps blood to the rest of the body and is the strongest chamber as it contracts most forcefully. There are also four valves in the heart that help to direct the blood flow [1].

#### *1.1.2 The conduction system*

Cardiac muscle cells are all electrically excitable and are capable of propagating action potentials. In a normal subject the cardiac impulse arises in the sinoatrial node (SA node), which is located near the entrance of the superior vena cava. This specialized tissue is the heart's "natural pacemaker". The rate of impulse formation can increase or decrease as sympathetic and parasympathetic nerve fibres end in this region causing the heart rate to vary.

After the initial impulse evolvment, action potentials spread from the SA node throughout the atria. Then, several pathways serve to channel the impulse from the SA node to the atrioventricular node (AV node). The AV node is normally the only conducting bridge between the atria and ventricles.

After emerging from the AV node the impulse finally enters the ventricular conduction system. The ventricular conduction system consists of the bundle of His, the right bundle branch, the left bundle branch and the Purkinje network. The latter is a network of nerve-like fibres that carry the electrical signal from the His bundle to

the heart muscle itself. Figure 1.1 illustrates the basic structure of the heart together with its conduction system, while figure 1.2 is a flow chart of the sequence of the normal cardiac activation [2].

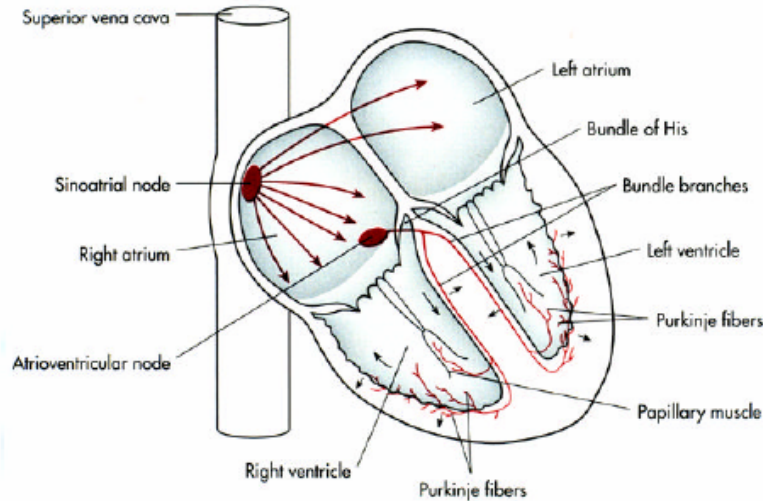


**Figure 1.1:** *The heart and its conduction system*

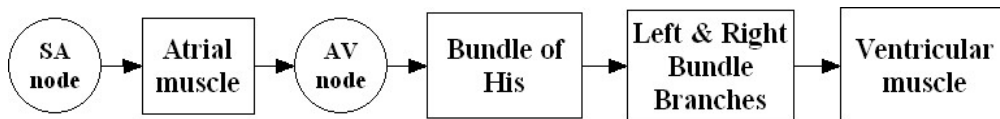


**Figure 1.2:** *Normal conduction pathway*

## **1.2 The electrocardiogram (ECG)**

### **1.2.1 The 12-lead ECG**

The electrical activity of myocardial cells establishes small currents within the body. These lead to potential differences on the surface, which can be detected using suitable equipment. The graphic record of these body surface potentials as a function of time is known as the electrocardiogram (ECG).

The ECG can be recorded by special medical devices, which are capable of recording the electrical activity of the heart from electrodes placed on the skin in specific locations. Modern ECG recorders utilize twelve leads, which are composed of three bipolar limb leads (*I*, *II*, *III*), three augmented unipolar limb leads ( $aV_R$ ,  $aV_L$ ,  $aV_F$ ) and six unipolar precordial leads ( $V_1$ ,  $V_2$ ,  $V_3$ ,  $V_4$ ,  $V_5$ ,  $V_6$ ).

The first three bipolar limb leads (*I*, *II*, *III*) use one limb electrode as the positive pole and another electrode as the negative pole. The positioning of them was first introduced by Eithoven as shown by the equilateral triangle called Eithoven's Triangle in the figure 1.3. These leads obey the following equation, which is known as the Eithoven's Law:

$$\text{Lead II} = \text{Lead I} + \text{Lead III} \quad (1.1)$$

The second three augmented unipolar limb leads ( $aV_R$ ,  $aV_L$ ,  $aV_F$ ) use one limb electrode as the positive pole (placed on the right arm, the left arm and the left foot, respectively) and the other electrodes are averaged together to create a composite negative reference (alternatively common ground can be used). They termed augmented because the potentials may be smaller than desirable so they are amplified. The last six unipolar precordial leads ( $V_1$ ,  $V_2$ ,  $V_3$ ,  $V_4$ ,  $V_5$ ,  $V_6$ ) are arranged laterally on right side of heart over the anterior apical portion of heart and then laterally on the left side of the heart as shown in figure 1.4. These leads measure the amplitude of the cardiac electrical current in an anterior-posterior aspect with regard to the heart as opposed to the limb leads, which record in the coronal plane [3].

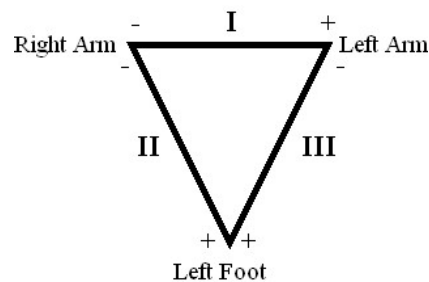


**Figure 1.3:** Eithoven's Triangle

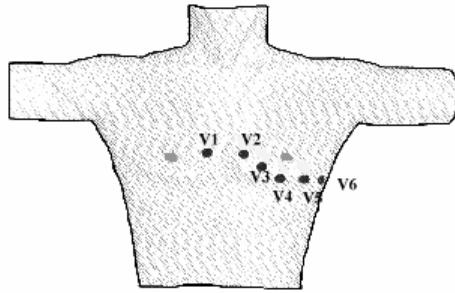


*Figure 1.4: Placement of the unipolar precordial leads*

### *1.2.2 ECG individual components*

A typical heart beat as recorded by lead II is illustrated in figure 1.5. Generally, it consists of a P-wave, a PR-interval, a QRS-complex, a ST-segment, a QT-interval and a T-wave. The P-wave refers to electrical currents produced in atria during depolarization and it initiates contraction of the atria. The PR-interval represents the atria to ventricular conduction time. The QRS-complex is the result of the production of electrical currents in ventricles during depolarization and it initiates ventricular contraction. The ST-segment is important in identifying pathology such as myocardial infarctions (elevations) and ischemia (depressions). The QT-interval expresses the duration of activation and recovery of the ventricular muscle. The T-wave occurs during ventricle repolarization. Note that multiple variations of the QRS-complex exist and some of them are presented in figure 1.6. The naming convention is performed as follows: The R-wave is the first (and the second) upward deflection of the QRS-complex, the Q-wave is the downward wave that precedes R-wave, while the S-wave is the downward deflection of the QRS-complex which follows R-wave [3].

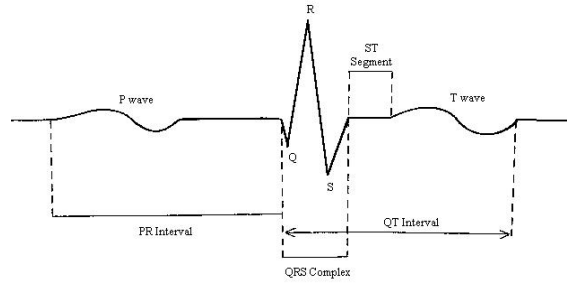


**Figure 1.5:** Individual components of a normal ECG beat (lead II)

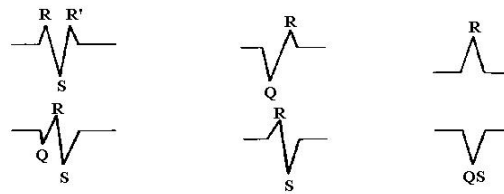


**Figure 1.6:** Some of the multiple variations of the QRS-complex

### 1.2.3 Heart rate (HR)

The heart rate (HR) is defined as the number of cardiac cycles that occurred in a minute. The cardiac cycle can be specified by the duration between two identical points of consecutive ECG waveforms such as the R-R interval. Therefore, the HR can be estimated by:

$$\text{HR} = \text{R-R intervals} / \text{Minute} \quad (1.2)$$

and is measured at beats per minute (bpm).

Usually, the HR is computed by the division of a minute to the time duration of a cardiac cycle (R-R interval). If the ECG recording speed is 25mm/sec, which is a universal standard, then a length equal to 1mm at the horizontal axis of the electrocardiographic map as shown in figure 1.7 corresponds to time duration of 0.04sec. Moreover, the vertical axis of the electrocardiographic map is also standardized and 1mm corresponds to 0.1mV of recorded voltage. Consequently, the

time duration of an R-R interval can easily be calculated in a similar manner to the HR by the following equation:

$$\text{HR} = 60 \text{ sec} / \text{R-R interval (sec)} \quad (1.3)$$

When the R-R intervals are not equal as for example in an atrial fibrillation a justifiable question could be how to estimate the cardiac cycle. In such situations the number of R-R intervals existing through the available length of the ECG recording should be counted. Then this number should be multiplied by a suitable factor in order to compute how many cardiac cycles occurred in a minute, thus calculating the HR. For example, if the available length of the ECG recording is six seconds, then after counting the different R-R intervals in these six seconds one should multiply by ten. Though for only three seconds available one should multiply by twenty and so on [3].

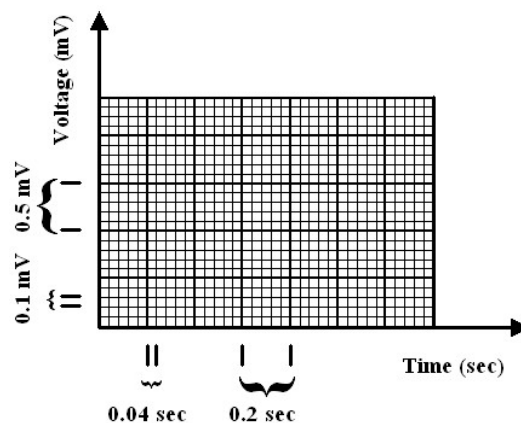


*Figure 1.7: Electrocardiographic map*

#### 1.2.4 Heart rhythm

The heart rhythm is characterized as sinus only when the two following conditions exist: An ECG recording every P-wave must be followed by a QRS-complex and simultaneously every QRS-complex must be preceded by a P-wave [3].

## *1.3 Arrhythmias*

### *1.3.1 Introduction*

Any turbulence in the heart rhythm is characterized as arrhythmia. Many different kinds of arrhythmias exist and their classification depends upon their origin. Therefore, there are arrhythmias originated from the SA node like sinus tachycardia and sinus bradycardia and arrhythmias induced by the atria like atrial premature contractions and atrial fibrillation. There are also arrhythmias caused by the AV node and the bundle of His like premature junctional contractions and arrhythmias introduced by the ventricles like premature ventricular contractions and ventricular tachyarrhythmia.

Cardiac arrhythmia is the leading cause of death in the Western world and strikes mostly people with a history of heart disease or damage resulting in sudden death but can also occur in young and apparently healthy men and women<sup>4</sup>. Furthermore, those with heart problems die usually due to an acute lethal arrhythmia rather than sudden deterioration of the heart [3,5].

### *1.3.2 Sinus tachycardia (ST)*

Sinus tachycardia (ST) occurs when the heart rate is greater than 100 beats per minute at rest although the rhythm is the same as the normal sinus rhythm. Many processes can result in the heart rate increasing at rest. Exercise, pregnancy and emotion can all result in sinus tachycardia. Sometimes sinus tachycardia may be adjusted compensatorily by the circulatory system via the sympathetic nervous system to some conditions. Such conditions include low blood pressure, low blood volume, impaired ability of the blood to transport oxygen, or ineffective ventricular ejection. Anaemia, post-surgical blood loss, heart failure and fever are situations when sinus tachycardia occurs clinically as a compensatory mechanism. Pain, cancer, endocrine disorders, and drug toxicity or drug withdrawal all of which are associated with abnormally

elevated energy expenditure can also result in sinus tachycardia. Drugs can also cause sinus tachycardia whereas sometimes the cause is unknown. Figure 1.8 illustrates an ECG signal during sinus tachycardia [3].

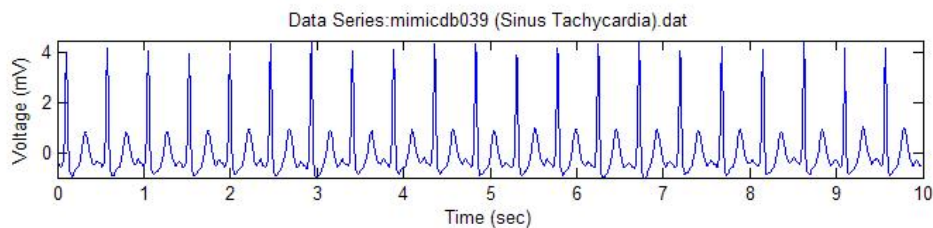


**Figure 1.8:** An ECG signal during sinus tachycardia

### 1.3.3 Sinus bradycardia (SB)

Sinus bradycardia (SB) occurs when the heart rate is lower than 50 beats per minute although the rhythm is the same as the normal sinus rhythm and is stimulated by an increased tone activity of the parasympathetic nervous system. This could be physiological if the subject is asleep, it is an athlete or a pregnant woman. However, there are many pathological causes that generate sinus bradycardia and some of them are very serious. These are increased endocranial pressure, imbalances of the carotid ventricle, hypothyroidism, arteriosclerosis of the elderly, S.S.S., heart attack, obstructive jaundice, recovery from infectious diseases and any drug consumption such as  $\beta$ -blockers.

One should be aware of sinus bradycardia for two reasons. Firstly, because the QT-interval is long and thus the “R on T phenomenon” is favoured. This phenomenon sets ventricular tachycardia, which is a critical type of arrhythmia. Secondly, in many cases sinus bradycardia appearance is accompanied with the development of S.S.S.. Figure 1.9 illustrates an ECG signal during sinus bradycardia [3].

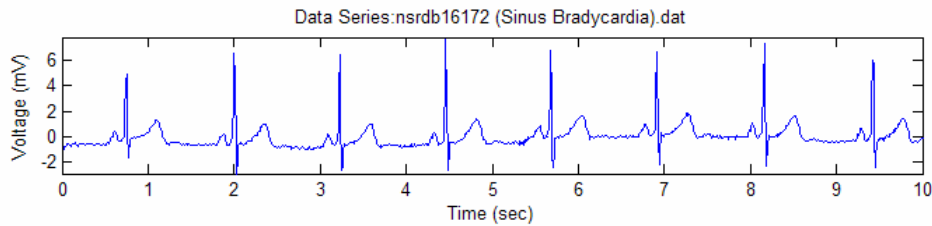


**Figure 1.9:** An ECG signal during sinus bradycardia

### 1.3.4 Premature contractions (PC)

Premature beats are the most common cause of an irregular heartbeat and occur earlier than expected interrupting the normal heart rhythm. Premature beats are often associated with other arrhythmias and tend to be more common in people with heart disease. They may originate from anywhere in the heart. Premature contractions in the ventricle (PVC = premature ventricular contraction) and in the atria (PAC = premature atrial contraction) are common.

Usually the presence of premature contractions in normal individuals does not require treatment unless they cause intolerable symptoms. Some changes in lifestyle, such as reducing stress or avoiding caffeine will often control them. In order to avoid serious implications a cardiologist should examine patients with PVC's when they are frequent or occur in certain patterns although treatment may not be needed. Those without heart abnormalities rarely have serious problems.

#### 1.3.4.1 Premature atrial contractions (PAC)

Premature Atrial Contractions (PAC) originate within the atrial myocardium but outside the SA node and occur before the next expected sinus discharge; it maybe conducted normally through the AV node and ventricles; or it can be partially or completely blocked. Although an increased rate of premature contractions occur before the onset of atrial fibrillation and are usually associated with lung and thyroid diseases, the cause of PAC is unknown. Figure 1.10 presents an ECG signal disturbed with one atrial premature contraction.

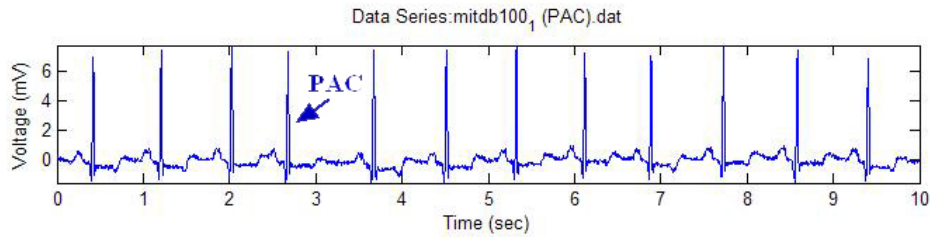


**Figure 1.10:** An ECG signal with an introduced PAC

#### 1.3.4.2 Premature ventricular contractions (PVC)

Premature Ventricular Contractions (PVC) arise from a ventricular focus with enhanced automaticity or may represent a form of reentry within the His-Purkinje system. PVC's are the most common of the ventricular arrhythmias and may occur randomly or may alternate with normal beats in a regular pattern. Isolated PVC in the setting of cardiac disease (e.g. recent heart attack) can indicate increased risk of having ventricular tachycardia or fibrillation, both of which increase the risk of sudden death. Figure 1.11 presents an ECG signal disturbed with one ventricular premature beat [3,5].

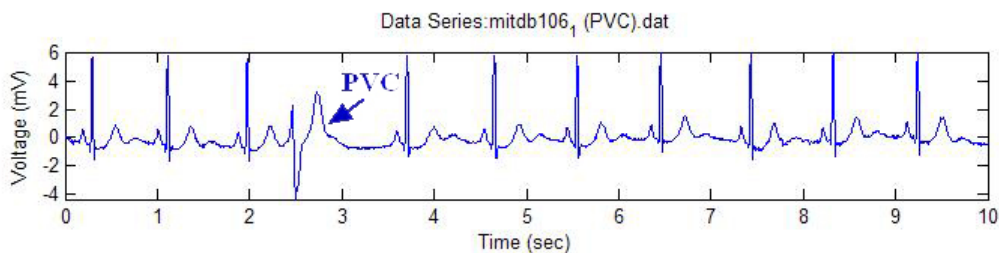


**Figure 1.11:** An ECG signal with an introduced PVC

#### 1.3.5 Atrial fibrillation (AF)

Atrial fibrillation is characterised by an irregularly erratic pulse and it is the most common abnormal heart rhythm. It is more common in older people and rare in children and adolescents. Its incidence increases with age and in the United States there are more than one and a half million sufferers<sup>4</sup>. The pulse rate can either be high

or low but in atrial fibrillation, the atrial and ventricular contractions are not synchronized together. The atria may be contracting at greater than 300-400 beats per minute. The electrical signals from the atria must pass through the AV node, which acts as a rate controlling device only allowing a certain number of electrical signals to pass to the ventricle per minute. As a result, the heart rhythm is irregular and erratic.

Atrial fibrillation can be variable and unpredictable and many people are asymptomatic. Episodes can last from minutes to hours, revert spontaneously, and recur infrequently and sometimes can result in a dominant atrial rhythm.

The basic cause of atrial fibrillation is unknown but is often associated with certain diseases. Such diseases include coronary heart disease, hypertension, mitral valve prolapse, congestive heart failure, rheumatic heart disease, cardiomyopathy, congenital atrial malformations, and metabolic diseases as well as alcohol and drug use - and also withdrawal - especially in the young and mid-adult years. Complications can occur which include serious circulatory problems, the risk of cerebral embolism and stroke. Atrial fibrillation shortens life expectancy and increases the risk of stroke particularly if the age is increased and cardiovascular disease is also present. Figure 1.12 illustrates an ECG signal during an atrial fibrillation episode [3,5].

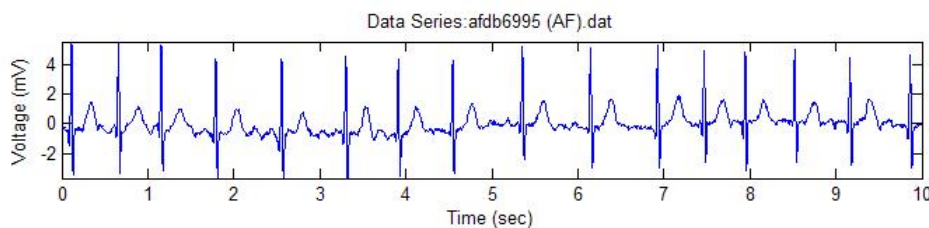


**Figure 1.12:** An ECG signal during an atrial fibrillation episode

### 1.3.6 Ventricular tachyarrhythmia (VT)

The ventricular tachyarrhythmias are fast heart rhythms (>100 beats per minute) that arise entirely within the lower chambers of the heart (the ventricles), include a number of different rhythms and can be life-threatening. VTs are divided into monomorphic

which would appear on an ECG record with a regular rate and rhythm and fixed shape or morphology of the ECG trace or polymorphic which is irregular in rate and rhythm and has varying shapes or morphologies on the ECG. Polymorphic ventricular tachycardia is the most dangerous rhythm with ventricular fibrillation being the worst form leading to death if not corrected.

In developed countries, the majority of the patients suffer from coronary artery disease. Although most patients having ventricular tachycardia will have underlying coronary disease or severely depressed heart function some have no demonstrable disease of the heart muscle or coronary arteries<sup>4</sup>.

#### *1.3.6.1 Monomorphic ventricular tachycardia*

Symptoms such as palpitations or shortness of breath can result from ventricular tachycardia in which the ventricle beats abnormally fast and inefficiently. Syncope or sudden death may result with faster heart rates and underlying heart disease. Rates between 110 and 150 beats per minute (bpm) may be tolerated, rates  $> 180$  bpm may cause drops in arterial pressure and syncope whereas rates  $> 220$  bpm are imminently dangerous. Figure 1.13 illustrates an ECG signal during a monomorphic ventricular tachycardia episode.

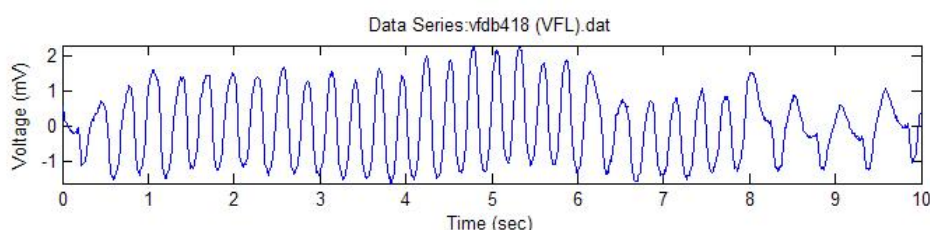


**Figure 1.13:** An ECG signal during a monomorphic ventricular tachycardia episode

#### *1.3.6.2 Polymorphic ventricular tachycardia: Ventricular fibrillation (VF)*

The mechanism of ventricular fibrillation is not known although it results when multiple sites in the ventricles fire impulses very rapidly in an uncoordinated fashion.

The ventricles stop the circulation of blood and death follows unless emergency treatment is given. VF causes death in patients with cardiac arrest and is most commonly associated with structural heart disease. Specifically, coronary artery disease and myocardial infarction or ischemia together with dilated cardiomyopathies are the most common underlying heart disease.

In episodes of cardiac failure, fibrillation is almost preceded by a run of ventricular tachycardia, which eventually gives way to the fibrillation itself. Therefore, any clinically useful detector should respond to the runs of tachycardia preceding fibrillation, since medical intervention is needed at the earliest opportunity. Figure 1.14 illustrates an ECG signal during a ventricular fibrillation episode [3,5].

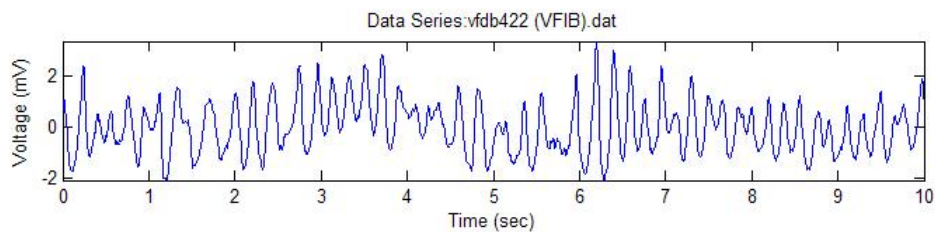


**Figure 1.14:** *An ECG signal during a ventricular fibrillation episode*

## 2. ALGORITHMS OVERVIEW

### 2.1 *Fourier transform*

#### 2.1.1 *Continuous-time Fourier transform (CFT)*

Amongst others, signal-processing field involves various feature extraction methods. These methods address the problem of extracting information from a given signal  $x(t)$  and converting it into a recognizable form. The most common approach to this issue is to transform  $x(t)$  to a different domain, where it is easier to interpret the signal. The latter procedure should be performed using an information-preserving mapping. The most popular method to implement this, perhaps, is the *Continuous-time Fourier Transform (CFT)*, which is defined as follows:

$$X(f) = \int_{-\infty}^{+\infty} x(t) \exp(-j2\pi ft) dt \quad (2.1)$$

and with its inverse transform:

$$x(t) = \int_{-\infty}^{+\infty} X(f) \exp(j2\pi ft) dt , \quad (2.2)$$

where  $X(f)$  is referred to as a spectral representation of the signal  $x(t)$  and  $f$  represents frequency, which is the new domain.

The CFT reveals how the energy in the signal  $x(t)$  is distributed with respect to the frequency. The main limitation of the CFT is that the values of the computed coefficients are affected by all the values of  $x(t)$  from  $t = -\infty$  to  $+\infty$ . Therefore, any particular feature in  $X(f)$  cannot be linked with a specific time region of  $x(t)$ . This is mentioned as lack of time resolution (See Appendix) and it means that although we

might be able to determine all the frequencies present in a signal, we do not know when they are present.

In many cases, the CFT is the most useful representation, especially when  $x(t)$  does not involve any special time variations. However, for many signals, the nature of  $x(t)$  varies with time. Consequently, in order to analyze this type of signals, a spectral representation that includes some explicit dependence on time is needed. This has led to the introduction of the *Short-Time Fourier Transform* [7,8].

### 2.1.2 Short-time Fourier transform (STFT)

The *Short-Time Fourier Transform* performs a spectral transformation of  $x(t)$  that informs us not only about which frequencies are present in the signal, but also when a particular frequency was present. In this approach, the frequency variable  $f$  defined by CFT is retained and a new one, the time variable  $\tau$ , is introduced. The latter variable ensures that only values of  $x(t)$  that are close to  $\tau$  would be able to influence the transform coefficients. This is achieved by multiplying the original signal by window functions localized at  $\tau$ . Thus, the two-variable STFT of signal  $x(t)$  is defined as:

$$X(f, \tau) = \int_{-\infty}^{+\infty} x(t) g^*(t - \tau) \exp(-j2\pi ft) dt, \quad (2.3)$$

where  $g^*(t - \tau)$  represents the complex conjugate of a window function that is localized around time  $t = \tau$ . If the window function is real then  $g^*(t - \tau) = g(t - \tau)$ . A typical choice for the window function is the Gaussian  $g(t - \tau) = \exp(-\beta(t - \tau)^2 / 2)$  since it falls away quickly to zero for times others than  $t = \tau$ . For this choice, the complex conjugate notation is removed from equation (2.3) since it is real. Apparently, if  $g(t) = 1$  the STFT in equation (2.3) reduces to the CFT given in equation (2.1).

Therefore, the primary purpose of the window in the STFT is to limit the extend of the signal to be transformed so that the spectral characteristics are reasonably stationary over the duration of the window. However, at the calculation of STFT any sharp change of the analyzed waveform  $x(t)$  around time  $t = \tau$  will not appear in the STFT solely at  $\tau$ , but it will rather spread over a region of time in the vicinity of  $t = \tau$ . The range of spread depends on the length of the applied window.

Apparently, as discussed previously, the more rapidly the signal characteristics alter, the shorter the window should be. Nevertheless, as the length of the window diminishes, frequency resolution (See Appendix) decreases. On the other hand, as the window becomes shorter, the ability to distinguish resolvable transitions with time increases. Conclusively, the choice of the window length becomes a trade-off between time resolution and frequency resolution.

The time and frequency resolution cannot be arbitrarily small since their product  $\Delta t \Delta f$  (known as the time-bandwidth product) is lower bounded.

$$\Delta t \Delta f \geq C \quad (2.4)$$

where  $\Delta t$  and  $\Delta f$  is the length of the window in time and frequency domain, respectively, and  $C$  is a nonzero constant which depends on the definition of the width of a selected function. Equation (2.4) is referred to as the uncertainty principle (or Heisenberg inequality), which states that the time resolution can only be improved at the expense of frequency resolution (or vice versa).

Once the window function  $g(t)$  is chosen the time and frequency resolutions of the STFT are fixed for all values of  $t$  and  $f$  since the same window is utilized throughout the transform. This characteristic of the STFT is shown schematically in figure 2.1. The tiles of the  $\tau - f$  plane represent regions where the basis functions  $g^*(\tau - \tau_i) \exp(-j2\pi f_j \tau)$  are concentrated. These regions are illustrated as rectangles of fixed area and dimensions for all values of  $\tau_i$  and  $f_j$  [7-9].

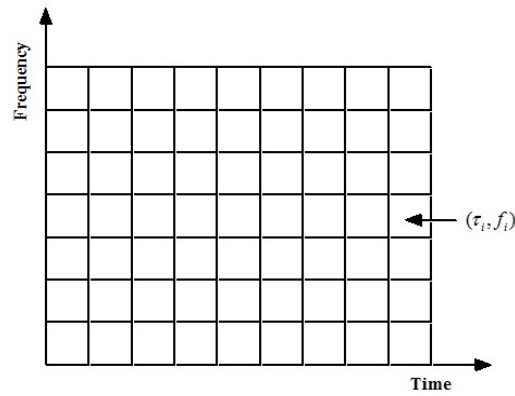


**Figure 2.1:** Time & frequency resolutions of STFT

## 2.2 Wavelet transform

### 2.2.1 Wavelets overview

Wavelets have increasingly being used over the past decade in many new fields including signal processing such as image compression, turbulence, human vision, radar and earthquake prediction. Wavelets were first developed independently in different scientific fields like mathematics, quantum physics, electrical engineering and seismic geology, but more recently an interchange between those areas has led wavelet applications into today's form. Nowadays, the applications of the wavelet theory in signal processing extend from speech analysis, medical imaging, theoretical mathematics and physics to data compression, communications, oil exploration and seismic sensing as well as sonar, weather forecasting, stock market modeling.

The main reason for wavelets almost complete dominance in the signal processing range from the time they first appear is their advantageous behavior over the well-known Fourier methods. This behavior mainly concerns the good time resolution at high frequencies and good frequency resolution at low frequencies. It also concerns the variety of wavelet functions are currently available hence the most appropriate may be chosen for the signal under investigation (In contrast Fourier analysis is restricted to one shape: the sinusoid). In addition, this superiority is especially obvious when the processing signal involves discontinuities and sharp spikes, that is when

having both short-term and relatively long-term characteristics. In order to understand wavelets together with their transform deeply it is better to take a closer look at what exactly wavelets are.

Wavelets are “little waves” as their name reveals. “Waves” because they have an oscillatory behavior and “little” because their amplitude quickly decays to zero in both directions (positive and negative). Figure 2.2, for example, shows a classical wavelet known as the “Morlet” wavelet in time and frequency domain.

The Morlet wavelet consists of a plane wave modulated by a Gaussian. The Morlet’s wavelet function is given by:

$$\psi_0(\eta) = \pi^{-1/4} e^{i\omega_0\eta} e^{-\eta^2/2} , \quad (2.5)$$

where  $\omega_0$  is the center frequency. In this project, this parameter is taken to be  $\omega_0 = 6$  . Usually the  $\omega_0$  is chosen such that the second maximum of the real part of the wavelet function  $\Re\{\psi_0(\eta)\}$  ,  $\eta > 0$  , is half the first one.

A candidate function to be a wavelet should satisfy the admissibility condition:

$$\int \frac{|\Psi(\omega)|^2}{|\omega|} d\omega < +\infty , \quad (2.6)$$

where  $\Psi(\omega)$  stands for the Fourier transform of  $\psi(t)$ . This condition implies that  $\Psi(\omega)$  vanishes at the zero frequency and so wavelets must have a band-pass like spectrum. This also means that the average value of the wavelet in the time domain must be zero and therefore it must be oscillatory. Therefore, a candidate function should satisfy both essential prerequisites of having zero mean and of being localized in both time and frequency space. The Morlet wavelet does not satisfy exactly the admissibility condition since  $\Psi(\omega)|_{\omega=0} \neq 0$  (equation (2.6)). However, its value at zero frequency is negligible and it does not present a problem in practice. In addition to this type of wavelet, which is the main complex wavelet used in this study, there

are many other wavelets such as the “Paul wavelet”, which is also complex and the “DOG wavelets” (derivatives of a Gaussian), which are real [10-13].

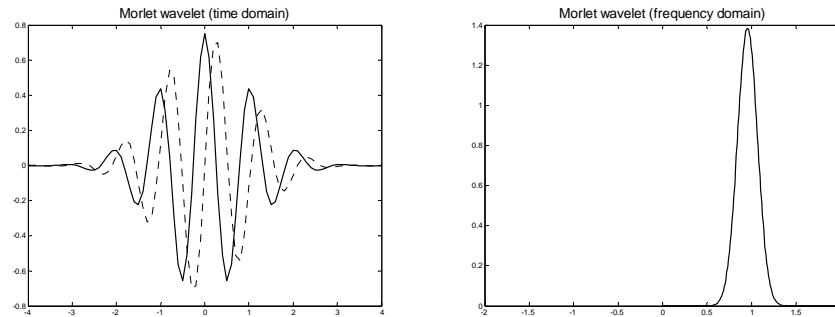


**Figure 2.2:** Morlet wavelet with  $\omega_0 = 6$  in time (left) and frequency (right) domain  
(Real part: solid line, Imaginary part: Dashed line)

### 2.2.2 Wavelet theory

Wavelet theory is a mathematical tool that can represent objects, actions or operations and can be applied almost anywhere. Like most tools, its primary purpose is to improve the efficiency of the analysis. Generally, the wavelet theory representations should not be blindly forced upon any application. This is because, although wavelet theory has some advantages over other traditional methods (i.e. Fourier) as mentioned previously, it should only be employed where its implementation could prove out to be beneficial.

Wavelet theory involves two primary operations: the scaling and the translation. Performing a combination of these two operations on a mother wavelet creates a set of scaled and translated version of this mother wavelet function, the wavelet set. When wavelet theory cuts up data into many interrelated components and these components are scaled and translated versions of a mother wavelet, then this breaking down process is called *wavelet transform*. The *wavelet transform* is generally an analysis filter. It examines or operates on the decomposed pieces instead of the original data set. The inverse process of putting these components back together in order to

reconstruct the original data is known as the *inverse wavelet transform*. The reconstruction formula is a synthesis filter. In this instant, a justifiable question could be why break a signal apart and then put it back together. The answer is because through the analysis process significant insights, gains and efficiencies can be obtained by operating on the separate pieces rather than the original signal. Nonetheless, some loss on information may occur during the inverse procedure of reconstruction of the initial data set. Usually, there is a trade off between the gains in efficiencies and the added distortion together with other losses. Each application has, of course, its own set of tradeoffs.

Overall, there are four primary wavelet transforms: The *continuous wavelet transform* (CWT) and the *wavelet series* (WS), the *discrete time wavelet transform* (DTWT) and the *discrete wavelet transform* (DWT). In the CWT and the WS the independent variable is continuous whereas in the DTWT and the DWT the independent variable is discrete. In the *wavelet series*, which is simply a sampled version of the CWT, and the DWT the transform domain parameters (the scale and the translation variables) are both discrete. In the DTWT, which corresponds to the CWT of a sampled sequence  $x_n = x(nT)$ , assuming sampling period to be unity leads us to consider only integer time shifts in the analysis, whereas the scale variable can vary continuously.

Depending on the nature of the analyzed signal (e.g. continuous-time or discrete-time signal) and the implementation method (e.g. by a computer) the choices of the available wavelet transforms are usually reduced to only two. For example if the analyzed signal is a sequence of the form  $x_n = x(nT)$  then our choices is either the DTWT or the DWT. Generally, the *continuous wavelet transform* is best suited for signal analysis. However, in the case where computer implementation is required the *continuous wavelet transform* is performed as described in the following section. On the other hand, its semi-discrete version (*wavelet series*) and its fully discrete one (*discrete wavelet transform*) have been used for signal coding applications, including image compression and various tasks in computer vision [11,13].

### 2.2.3 Continuous wavelet transform (CWT)

Assume the case of a signal with a mixture of short-lived high-frequency components that are closely spaced in time together with long-duration low-frequency components that are closely spaced in frequency. This type of signal does not comprise an exception but rather the majority of analysed signals. A suitable transform in this case would have sufficient time resolution to distinguish the brief high-frequency events, and at the same time, enough frequency resolution to separate the closely spaced low-frequency components. As mentioned above these two aims are incompatible with the STFT since the time and frequency resolutions are both fixed.

One possible solution to this problem is the use of a representation that has variable time-frequency resolution over the  $(\tau, f)$  plane. This representation should be chosen in such a way that it provides good time resolution at high frequencies and good frequency resolution at low frequencies. One such representation is the *continuous wavelets transform* (CWT), which is expressed as:

$$X(s, \tau) = \frac{1}{\sqrt{|s|}} \int_{-\infty}^{+\infty} x(t) \psi^* \left( \frac{t - \tau}{s} \right) dt \quad (2.7)$$

or as a convolution in the time domain:

$$X(s, \tau) = \frac{1}{\sqrt{|s|}} \left[ x(\tau) * \psi \left( \frac{-\tau}{s} \right) \right], \quad (2.8)$$

where  $t$  and  $\tau$  are time variables,  $x(t)$  is the time waveform being analyzed,  $\psi(t)$  is the mother wavelet function, and  $s$  is the variable known as scale. In equation (2.8) the sign  $*$  denotes the convolution operation. The term  $\frac{1}{\sqrt{|s|}}$  performs energy normalization, thus it keeps the energy of the scaled mother wavelet equal to the energy of the original mother wavelet.

The parameter scale  $s$  is similar to the scale used in maps. As in the case of maps, high scales correspond to a non-detailed global view of the signal and low scales correspond to a detailed view. Similarly, in terms of frequency, low frequencies (high scales) correspond to a global information of a signal that usually spans the entire signal, whereas high frequencies (low scales) correspond to a detailed information of a hidden pattern in the signal that usually lasts a relatively short time. Scaling, as a mathematical operation, either dilates or compresses a signal. Larger scales correspond to dilated (or stretched out) signals and small scales correspond to compressed signals. Figure 2.3 illustrates the scaling operation when applied to the Morlet mother wavelet with  $\omega_0 = 6$  .

The CWT is strictly defined as a time-scale representation. However, it often proves easier to interpret CWTs in terms of time and frequency rather than time and scale. Therefore, for a given wavelet the mapping  $f = K/s$  is possible to be used allowing the CWT of a signal to be interpreted in terms of frequency rather than scale. In order to examine the above relationship the method of [14] should be followed which is described in the implementation section.

For a better understanding of the differences between the STFT and the CWT let's consider equation (2.8), which is the formulation of the CWT as a convolution in the time domain. As with the STFT, the value of  $x(t)$  at  $t = \tau_0$  is smeared over a time equal to the width of the function  $\psi(\tau/s)$  . The width of a function can be defined in many ways; in this project, the width of a wavelet function is defined as the e-folding time of the wavelet amplitude (See Appendix). For the STFT case recall that the range of spread depends on the length of the applied window, which is fixed upon the selection of the window. In the CWT case, however, the width of  $\psi(\tau/s)$  is not fixed. It depends on the value of scale  $s$  . For example,  $\psi(2t)$  has half the width of  $\psi(t)$  , while  $\psi(t/2)$  has twice the width of  $\psi(t)$  (Figure 2.3). The larger the value of  $s$  , the wider the function  $\psi(\tau/s)$  would be. Since time resolution depends on the width of this function, the following situation obtains: as  $s$  decreases,  $\psi(\tau/s)$  becomes narrower in time so that the time resolution improves. Conversely, as  $s$  increases, the

time resolution is degraded. At the same time, the frequency resolution is enhanced because the quantity  $\Delta t \Delta f$  must be maintained constant.

Figure 2.4 shows the tiling of the time-frequency (time-scale) plane by CWT with rectangles centered at  $(\tau_i, f_j)$ . These rectangles represent regions where the functions  $\psi^*([\tau - \tau_i]/s_j)$  are concentrated, with  $f_j = K/s_j$ . As one can notice, the rectangles are of fixed area but variable shape. More analytically, at low frequencies (large scales) the rectangles are broad in time but narrow in frequency, since then the time resolution is poor and the frequency resolution is good. The converse is true at high frequencies (small scales) [8,11-14].

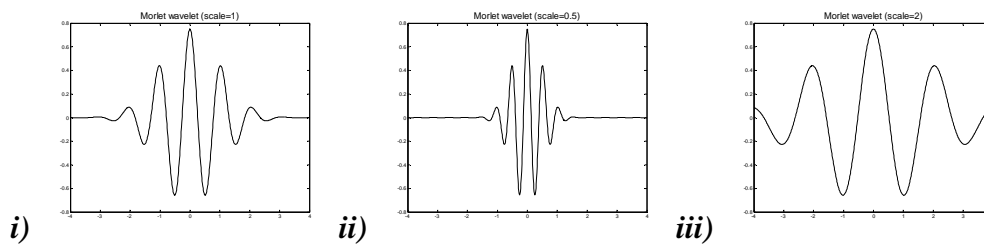


**Figure 2.3:** The scaling operation. i) Morlet mother wavelet with  $\omega_0 = 6$  (scale=1), ii) Morlet wavelet with  $\omega_0 = 6$  (scale=0.5), iii) Morlet wavelet with  $\omega_0 = 6$  (scale=2)

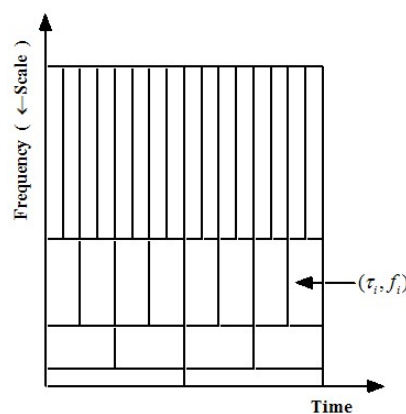


**Figure 2.4:** Time & frequency resolutions of CWT  
(the ratio used is illustrative)

#### 2.2.4 CWT versus STFT

As pointed out in the preceding paragraphs, a very basic distinction between wavelet transforms and Fourier methods, like STFT, is that while the basic functions of the latter consist of a function of constant width, the former has a frequency-dependent (actually scale-dependent) width. In other words, it is narrow at high frequencies and broad at low frequencies. This gives to the *wavelet transform* the ability to “zoom-in” on transitory phenomena, which usually are short-lived components of a signal. Another key distinction is that a variety of wavelet functions is currently available hence the most appropriate may be chosen for the signal under investigation.

It is apparent from the foregoing discussion that the CWT and the STFT have different frequency - and time - resolution properties. It is these properties, and their relationship to the characteristics of the signal itself, that determine the relative advantages of the two techniques for analysing a given signal. Consequently, the CWT is a preferred tool when the analysis requires good frequency resolution at low frequencies together with good time resolution for impulsive (high-frequency) events. The STFT is appropriate when the required frequency resolution (and time resolution) remains fixed across the time-frequency plane.

#### 2.2.5 Discrete wavelet transform (DWT)

As a transform of its own, the *discrete wavelet transform* (DWT) is mainly applicable in the image compression (in a two-dimensional form). The DWT is similar to WS but applies to discrete-time signals, thus both its independent variable and its transform variables are discrete. This section only addresses the special case of discrete wavelet transforms, which only allow scales that are powers of two and integer translations.

In this DWT, filters of different cutoff frequencies are used to analyze the sequence at different scales. The decomposition procedure in the DWT is simply obtained by successive filtering of the time domain sequence. The original sequence  $x_n$  is first

passed through a halfband lowpass filter  $g(n)$  and a halfband highpass filter  $h(n)$ . After the filtering, the sequence is subsampled by two, simply by discarding every other sample, because half of the samples can be eliminated according to the Nyquist's rule. The output of the highpass filter followed by subsampling constitutes one level of DWT coefficients. This comprises one level of decomposition. The filtering operation halves the width of the lowband (or the highband), thus it doubles the frequency resolution (after the filtering operation the frequency band of the sequence spans only half the previous frequency band). The subsampling by two operation doubles the scale but also halves the time resolution since only half the number of samples now characterizes the entire sequence.

The above procedure is repeated for further decomposition until two samples are left. Therefore, the output of each highpass filter followed by subsampling constitutes the corresponding level of DWT coefficients, while the subsampled output of the lowpass filter is passed through the lowpass and highpass filters for further decomposition. At each level, the filtering and subsampling will result in half the number of samples (and hence half the time resolution) and half the frequency band spanned (and hence double the frequency resolution). Figure 2.5 illustrates a basic computational cell of the DWT whereas figure 2.6 shows the overall organization of the DWT.

If the main information of the initial signal lies within the high frequencies, as happens most often, the time localization of these frequencies will be more precise, since they are characterized by more number of samples. If the main information lies only at very low frequencies, the time localization will not be very precise, since few samples are used to express signal at these frequencies. This procedure in effect offers a good time resolution at high frequencies and good frequency resolution at low frequencies as it would be expected.

The lowpass filters utilized in the DWT correspond to the scaling sequences, while the highpass filters are associated with the wavelet sequences. These filters should meet some specific constraints in order to accomplish perfect reconstruction of the initial sequence. The easiest case of achieving a perfect reconstruction appears when

the analysis and synthesis filters are identical (except for a time reversal). In this case, the impulse responses of the lowpass and highpass filters are related by:

$$h(L-1-n) = (-1)^n g(n) \quad (2.9)$$

where  $g(n)$  and  $h(n)$  are the lowpass and highpass filters respectively and  $L$  is the filter length in number of points, which has to be even.

The two filtering and subsampling operations can be expressed as:

$$y_0(k) = \sum_n x(n)g(-n+2k) \quad (2.10)$$

$$y_1(k) = \sum_n x(n)h(-n+2k) \quad (2.11)$$

where  $y_0(k)$  and  $y_1(k)$  are the subsampled by two outputs of the lowpass and highpass filters respectively.

Apart from these filters, it is possible to find others that provide perfect reconstruction using other constraints concerning the analysis and synthesis filters. The most famous are the ones developed by Daubechies, the Daubechies' wavelets [8,11,13,15].

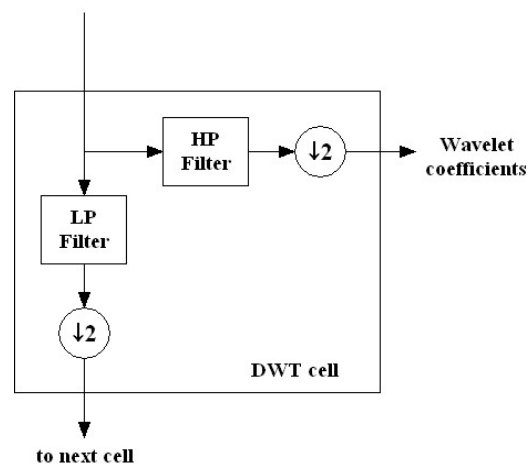


**Figure 2.5:** Basic computational cell of the DWT

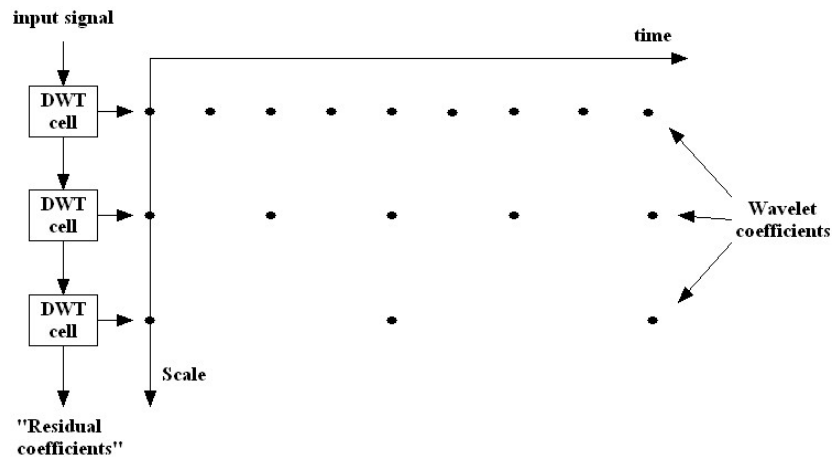


*Figure 2.6: DWT structure*

### 2.2.6 CWT versus DWT

As pointed out in previous sections, the CWT is computed by changing the scale of the wavelet function, shifting the wavelet function in time, multiplying by the signal, and integrating over all times. In the DWT case, filters of different cutoff frequencies are used to analyze the sequence at different scales. The sequence is passed through a series of highpass filters to analyze the high frequencies, and it is passed through a series of lowpass filters to analyze the low frequencies. The resolution of the sequence is changed by the filtering operations, while the scale is changed by upsampling and subsampling operations.

From the above, one can extract the following conclusions. The CWT together with its sampled version, the WS, provide highly redundant information as far as the reconstruction of the signal is concerned. This redundancy also requires a significant amount of computation time and resources. On the other hand, the CWT is often easier to interpret since its redundancy tends to reinforce the traits and makes all information more visible. This is especially true of very subtle information. Consequently, the CWT gains in "readability" and in ease of interpretation what it loses in terms of computational time and space saving.

However, the DWT is sufficient for exact reconstruction of the initial signal, if some special conditions hold, as discussed in the above paragraphs. Moreover, it ensures space-saving coding and it uses less computational time and resources when compared to those needed by CWT. Conclusively, the CWT is best suited to signal analysis whereas the DWT is, for example, more suitable for signal coding applications.

## 3. IMPLEMENTATION

### *3.1 Data acquisition*

The data set used in this project is a combination of seven different databases organized by PhysioBank<sup>6</sup>. PhysioBank is a large archive of well-characterized digital recordings of physiologic signals and related data for use by the biomedical research community and is available online. The data analysed in this study are part of the following databases: The MIT-BIH Normal Sinus Rhythm Database, the MIMIC Database, the MIT-BIH Arrhythmia Database, the MIT-BIH Atrial Fibrillation Database, the AF Termination Challenge Database, the MIT-BIH Malignant Ventricular Arrhythmia Database and the Creighton University Ventricular Tachyarrhythmia Database.

Each database includes excerpts of digitized long-term recordings of human subjects. The leads used are commonly two or more and the sampling frequency of each database is illustrated in table 3.1. In this case only ten seconds of a lead of each recording were analysed. Some of these recordings were obtained from subjects who experienced episodes of atrial fibrillation or ventricular tachyarrhythmia. Other subjects presented atrial or ventricular (or both) premature contractions during the ECG recording. Some other exhibited sinus tachycardia, while few subjects had no significant arrhythmias or were normal.

In order to have the same desirable time duration (of ten seconds) for the analysis all the recordings acquired in a renormalized form. Thus, the number of samples for each signal was different and it was dependent on its sampling frequency. Most of the available recordings were annotated. The residuals were classified by a cardiologist thus all the signal archives used were initially diagnosed. Based on the characteristics of each recording the data series are organized into various categories. Table 3.1 summarizes the number of signals used from each database, its characteristics and the sampling frequency of each database.

<b>Database</b>	<b>Signals</b>	<b>Characteristics</b>	<b>Sampling Rate</b>
<i>MIT-BIH Normal Sinus Rhythm</i>	<i>17</i>	<i>NSR</i>	<i>128</i>
	<i>1</i>	<i>Sinus Tachycardia</i>	
<i>MIMIC</i>	<i>7</i>	<i>NSR</i>	<i>125</i>
	<i>4</i>	<i>Sinus Tachycardia</i>	
<i>MIT-BIH Arrhythmia</i>	<i>18</i>	<i>Premature Contractions</i>	<i>360</i>
<i>MIT-BIH Atrial Fibrillation</i>	<i>10</i>	<i>Atrial Fibrillation</i>	<i>250</i>
<i>AF Termination Challenge</i>	<i>30</i>	<i>Atrial Fibrillation</i>	<i>128</i>
<i>MIT-BIH Malignant Ventricular Arrhythmia</i>	<i>29</i>	<i>Ventricular Tachyarrhythmias</i>	<i>250</i>
<i>Creighton University Ventricular Tachyarrhythmia</i>	<i>33</i>	<i>Ventricular Tachyarrhythmias</i>	<i>250</i>

**Table 3.1:** Signals and its characteristics

## 3.2 Data analysis

### 3.2.1 Pre-processing

Firstly, the initial sequence  $x_n$  was normalized by its standard deviation. This was not necessary, but makes it easier to compare between different wavelet transform results. One could instead normalize the wavelet transform but it is more efficient to normalize the time series since this is just an one-dimensional array [12].

### 3.2.2 Wavelet transform (WT)

Every time series  $x_n$  with  $n = 0 \dots N - 1$  belonging to the same database has the same time spacing  $\delta t$ , which is the inverse of sampling rate, and thus the same length  $N$ . As it is well-known, the *continuous wavelet transform* of a discrete sequence  $x_n$  (DTWT) is defined as the convolution of  $x_n$  with a scaled and translated version of a given mother wavelet  $\psi_0(\eta)$  as follows:

$$W_n(s) = \sum_{n'=0}^{N-1} x_{n'} \psi^* \left[ \frac{(n'-n)\delta t}{s} \right], \quad (3.1)$$

where superscript “\*” denotes a complex conjugate. The scaled and shifted version of the mother wavelet was normalized to have a unit energy at each scale (that is why the subscript 0 on  $\psi$  is dropped). The normalization process was performed to ensure that the wavelet transforms at each scale  $s$  were directly comparable to each other and to the transforms of a different time series.

Equation 3.1 was not used in its initial form for the computation of the wavelet transform, as it was considerably faster to perform the calculations in Fourier space. To approximate the CWT, the convolution in equation 3.1 was done  $N$  times (arbitrary choice) for each scale, where  $N$  was the number of points in the time series. These  $N$  convolutions were performed simultaneously in Fourier space using a discrete Fourier transform (DFT). The *DFT* of  $x_n$  is given by:

$$\hat{x}_k = \frac{1}{N} \sum_{n=0}^{N-1} x_n e^{-2\pi i k n / N}, \quad (3.2)$$

where  $k = 0 \dots N - 1$  is the frequency index. Therefore, according to the convolution theorem, the wavelet transform is the inverse of the product:

$$W_n(s) = \sum_{k=0}^{N-1} \hat{x}_k \hat{\psi}^*(s\omega_k) e^{i\omega_k n \delta t}, \quad (3.3)$$

where the angular frequency  $\omega_k$  is defined as:

$$\omega_k = \begin{cases} \frac{2\pi k}{N\delta t}, k \leq \frac{N}{2} \\ -\frac{2\pi k}{N\delta t}, k > \frac{N}{2} \end{cases} \quad (3.4)$$

Consequently using equation 3.2 and a standard Fourier transform routine, the DTWT can be calculated for a given scale  $s$  at all  $n$  simultaneously and efficiently.

In our implementation the Morlet wavelet was chosen with  $\omega_0 = 6$  to perform the transform while the scales  $s$  were chosen arbitrarily to be fractional powers of two:

$$s_j = s_0 2^{j\delta j}, \quad j = 0, 1, \dots, J \quad (3.5)$$

$$J = \delta j^{-1} \log_2(N\delta t / s_0), \quad (3.6)$$

where  $s_0$  is the smallest resolvable scale,  $J$  determines the largest scale and  $\delta j$  is the spacing between the discrete scales. The  $s_0$  was chosen so that the equivalent Fourier period is approximately  $2\delta t$ , since the smallest scale that can be resolved is approximately equal to the Nyquist frequency. The choice of a sufficiently small  $\delta j$  depends on the width of the wavelet function. For the Morlet wavelet, for example, a  $\delta j$  of about 0.5 is the largest value that still gives adequate sampling in scale whereas for other wavelet functions a larger value can be used. Smaller values of  $\delta j$  give a finer resolution. In this study, the value of 0.25 was used for  $\delta j$  and it appeared adequate to provide sufficient information.

Before we proceed to the next implementation steps of the data processing is necessary to mention some influence issues first. As we are dealing with finite-length time series errors will occur at the beginning and at the end of the wavelet power spectrum. This effect is caused by the assumption of the Fourier transform in equation 33 that the data is cyclic. To overcome this the time series was padded with sufficient

zeroes to bring the total length  $N$  up to the next higher power of two, thus limiting the edge effects and simultaneously speeding up the Fourier transform. However, at the same time the process of padding with zeroes introduces discontinuities at the end-points and, as the scale becomes larger, the amplitude decreases near the edges as more zeroes enter the analysis. The *cone of influence* (COI) is the region of the wavelet power spectrum,  $|W_n(s)|^2$ , in which edge effects become important. The COI is defined as the e-folding time for the autocorrelation of wavelet power at each scale. For minimal edge effects the e-folding time was chosen so that the wavelet power for a discontinuity at the edge drops by a factor  $e^{-2}$ . Note that the *COI* does not exist for cyclic series hence there is no need to pad this kind of data with zeroes.

Another arising issue is the interconnection between the wavelet scale and the Fourier frequency. The relation between them is not necessarily straightforward. Some wavelets, for example, are highly irregular without any dominant periodic components. In such cases, it is meaningless to try finding any equation that connects them. However, in the case of the Morlet wavelet it seems more reasonable.

As examination of the above relationship is required the method of [3] should be followed. Therefore, the equivalent Fourier period with respect to the wavelet scale can be analytically derived for a particular wavelet function after following the next steps:

- 1) Choose the desirable wavelet function,
- 2) Perform the wavelet transform of a cosine wave of a known frequency using equation 3.3 and the chosen wavelet function,
- 3) Compute the wavelet power spectrum,
- 4) Find the scale  $s$  at which the wavelet power spectrum reaches its maximum.

The resulting equation is a linear relation between wavelet scale and Fourier wavelength  $\lambda$  as given by:

$$s = \left[ \frac{\omega_0 + (2 + \omega_0^2)^{1/2}}{4\pi} \right] \lambda \quad (3.7)$$

For the Morlet wavelet with  $\omega_0 = 6$  the above process gave a value of

$$\lambda = 1.03s \quad (3.8)$$

for the equivalent Fourier period. This last equation indicates that for the Morlet wavelet the wavelet scale is almost equal to the Fourier period. An analogous procedure could be followed in the *discrete wavelet transform* case [12,14].

The software that calculates the *continuous wavelet transform* of a discrete sequence (DTWT) was based on routines originally came from [12] and were properly modified.

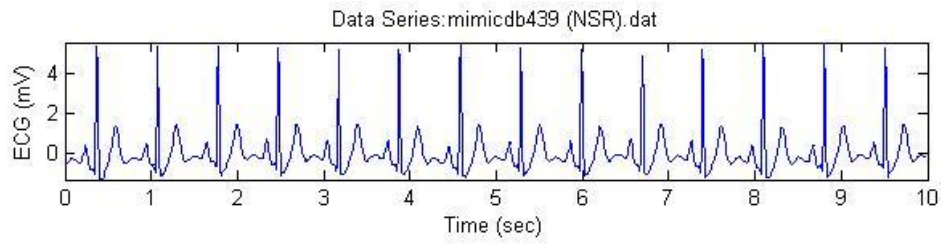
### 3.2.3 Post-processing

#### 3.2.3.1 Wavelet power spectrum (WPS)

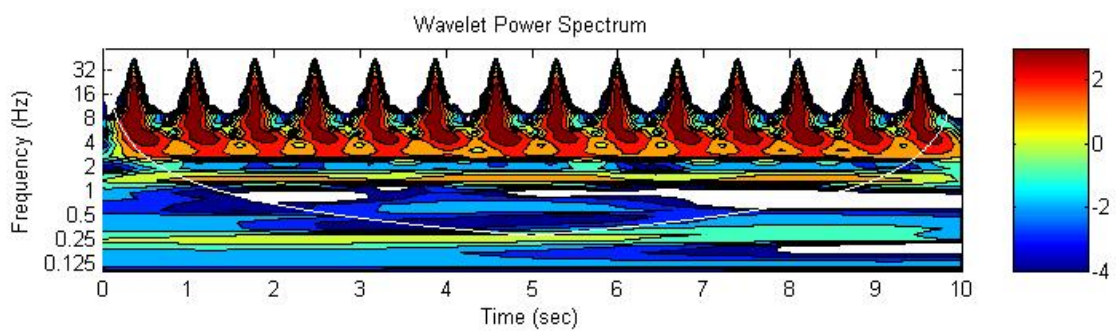
After the computation of the DTWT using the above described routines the amplitude of the transform  $|W_n(s)|$  was squared in order to produce the *wavelet power spectrum* of the initial data series  $|W_n(s)|^2$ . Basically, the *wavelet power spectrum* shows the distribution of the power of the signal in the time-scale (or time-frequency) plane.

Figure 3.1 illustrates a normal ten-second ECG signal (mimicdb439 (NSR).dat) and figure 3.2 its *wavelet power spectrum* (WPS). In the WPS the horizontal axis represents time while the vertical axis represents the equivalent Fourier frequency. The different colours represent the different levels of wavelet power. Therefore, the brown and the red regions refer to high power while the cyan and the blue ones refer to lower power. The white curved line appearing at the bottom of the WPS determines

the boundaries of the COI region, thus underneath this line the edge effects become important [12].



**Figure 3.1:** A normal ECG signal



**Figure 3.2:** Wavelet Power Spectrum of the normal ECG signal of figure 3.1

### 3.2.3.2 Global wavelet spectrum (GWS)

A vertical slice through a wavelet plot is a measure of the local spectrum. Accordingly, a time-average over the whole *wavelet power spectrum* produces the *global wavelet spectrum* (GWS) which is given by:

$$\overline{W^2}(s) = \frac{1}{N} \sum_{n=0}^{N-1} |W_n(s)|^2 \quad (3.9)$$

Consequently, after the calculation of the *wavelet power spectrum* the computation of the GWS was performed. Figure 3.3 shows the *global wavelet spectrum* of the same transformed signal (mimicdb439 (NSR).dat) [12].

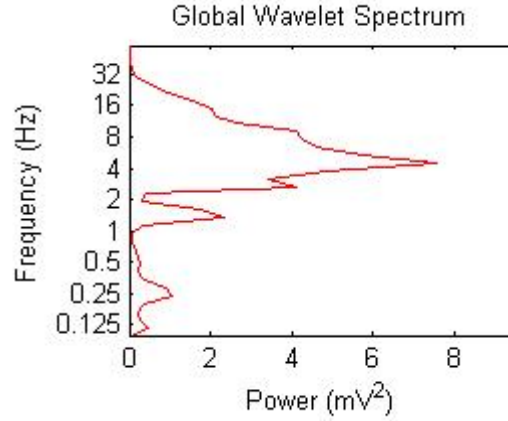


**Figure 3.3:** Global Wavelet Spectrum of the normal ECG signal of figure 3.1

### 3.2.3.3 Scale-averaged wavelet power spectrum (SAWPS)

Generally, the *scale-averaged wavelet power spectrum* (SAWPS) examines the fluctuations in power over a range of scales. It is defined as the weighted sum of the *wavelet power spectrum* over scales  $s_1$  to  $s_2$  :

$$\overline{W_n^2} = \frac{\delta j \delta t}{C_\delta} \sum_{j=j_1}^{j_2} \frac{|W_n(s_j)|^2}{s_j} \quad (3.10)$$

where the range  $[s_1 s_2]$  determines the band of scales in which equation 3.10 is applied. Therefore, specific interesting bands of scales can be isolated within the WPS and their power fluctuations can be studied.

The factor  $C_\delta$  comes from the reconstruction of a  $\delta$  function from its wavelet transform  $W_\delta(s)$  using the wavelet function  $\psi_0(\eta)$  :

$$C_\delta = \frac{\delta j \delta t^{1/2}}{\psi_0(0)} \sum_{j=0}^J \frac{\Re\{W_\delta(s_j)\}}{s_j^{1/2}} \quad (3.11)$$

where  $\Re\{W_\delta(s_j)\}$  represents the real part of the wavelet transform of the delta function. The  $C_\delta$  is scale independent and is a constant for each wavelet function. For the Morlet wavelet with  $\omega_0 = 6$  it is equal to 0.776.

Figure 3.4 illustrates the *scale-averaged wavelet power spectrum* over a band of scales of the normal ECG signal of figure 3.1. It can be noticed that every power peak shown at the SAWPS corresponds to a peak of the ECG signal. This is an intrinsic consequence as this spectrum represents the power fluctuations with respect to time duration [12].

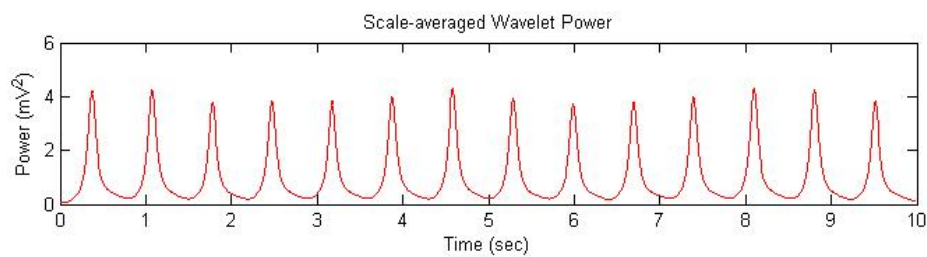


**Figure 3.4:** *The scale-averaged wavelet power over a band of scales of the normal ECG signal of figure 3.1*

### 3.2.3.4 GWS analysis

It was noticed that the GWS was a constitute of several power peaks. These maxima determine some frequency bands with close power values. In order to distinguish these bands the next procedure must be followed, which is also illustrated graphically in figure 3.5. The resultants frequency bands helped in the estimation of the variables discussed in the following section.

1. Compute the *global wavelet spectrum* (GWS)
2. Reject some low frequencies in the GWS that are below a user defined threshold. This is performed due to the COI existence (here taken to be equal to one)

3. Find all the local maxima within the GWS
4. For each computed local maxima
  - a. Find the local minimum at the left
  - b. Find the local minimum at the right
  - c. Keep the local minimum with the largest power amplitude as the first boundary of the band
  - d. Find the second boundary that is adjacent on the other side of the maximum and has the same power with the first one
  - e. These two boundaries determine one band
5. Repeat the above procedure for all local maxima in order to calculate all the frequency bands within the GWS

Algorithm for computing frequency bands in GWS

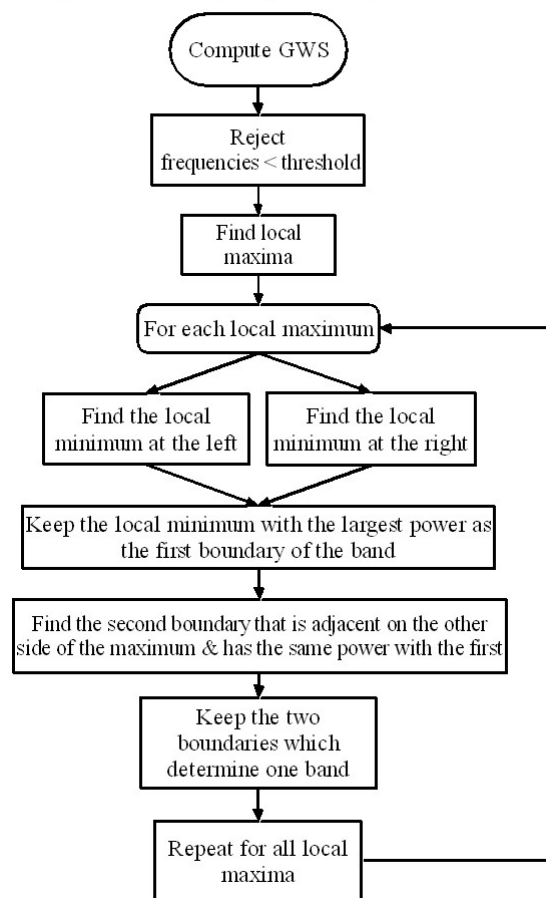


**Figure 3.5:** Flow diagram of the computation of the frequency bands within GWS

### 3.2.3.5 VT detection

The terminology “ventricular tachyarrhythmias” usually includes two main subcategories. These are the monomorphic ventricular tachycardia (figure 1.13) and the ventricular fibrillation (figure 1.14). Generally, it was observed that in ventricular tachyarrhythmias the GWS had a special characteristic in the frequency domain that was absent in atrial fibrillation or other types of arrhythmia. This characteristic was presented as a thin high power band in the WPS and it was usually obvious within the interval 2.5 - 5.5 Hz. As a result, this particular feature was reflected a dominant narrow but with high power frequency band in the GWS. The other frequency bands within the GWS were usually wider and with much lower power. This specific frequency band was defined as “band of interest”. Figure 3.6 shows the *global wavelet spectrum* of an ECG signal recorded during a ventricular tachycardia episode (vfdb423 (VT).dat). Compare this GWS with the one illustrated in figure 3.3. The latter even if it has a high power frequency band it is not narrow and it also has other two bands with not negligible power. Remember that at frequencies below approximately one Hertz the wavelet transform was highly affected by side effects so these values were discarded.

In order to distinguish the ECG data series comprising ventricular tachyarrhythmia episodes from the other characterized with different arrhythmias four different parameters were introduced. The first one, “*potential\_vt*”, regards the presence (or not) of the peak of the highest power frequency band within the interval [2.5-5.5] (Hz). If the peak of the highest power frequency band concerns amongst the latter boundaries then the variable is set equal to “yes”. This denotes that the possibility of the existence of a ventricular tachyarrhythmia episode is high. The second parameter that was checked is called “*peak\_diff*”. This variable is equal to the difference between the power amplitudes of the two maximum peaks of the limited GWS. It indicates how far away from the “band of interest” is the second higher power band. The third parameter refers to the width of the “band of interest” and is called the “*boi\_width*”. This width is defined in this case as an analogous of the e-folding time of an oscillation thus it is equal to the time needed for the maximum of the “band of interest” to decrease down to the 1/e of its value. The last variable is not a primary variable. However it is very helpful as it provides the right classification of some

ambiguous cases. Remember the fact that ventricular tachyarrhythmias introduce high power peak within the GWS. This characteristic was measured with the help of “*power\_fr*”, which represents the power fraction of the “band of interest” within the GWS.

Depending on the values of the above parameters it was possible to distinguish between the ECG data series with ventricular tachyarrhythmia. This classification process was performed by following the decision flowchart, which is analytically described in figure 3.7. A more concise version of this classification algorithm follows. Thus:

- 🖼️ If the “*potential\_vt*” is false, then the algorithm seeks for missed VT detections concerning high power bands outside the predefined range [2.5-5.5 Hz] . This is performed by evaluating both “*peak\_diff*” and “*boi\_width*” towards some predefined thresholds.
  
- 🖼️ If the “*potential\_vt*” is true, then the rest variables are assessed starting from “*peak\_diff*”. In the case of ambiguous situations (AS) the variables are evaluated hierarchically starting from “*peak\_diff*”, continuing with “*boi\_width*” and concluding with “*power\_fr*”. For example, if “*peak\_diff*” < ‘7’ then the control is ended since the possibility of the existence of any VT is very small. On the other hand, if ‘7’ <= “*peak\_diff*” <= ‘15’ (AS) then the “*boi\_width*” is assessed and if “*boi\_width*” <= ‘1.2’ (AS) then the “*power\_fr*” is evaluated and its value determines the final decision which is the existence or not of any VT.

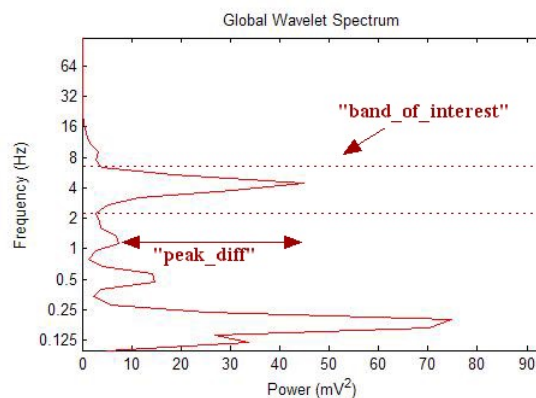


**Figure 3.6:** Global Wavelet Spectrum of a ventricular tachycardia ECG signal

Algorithm for the detection of Ventricular Tachyarrhythmias

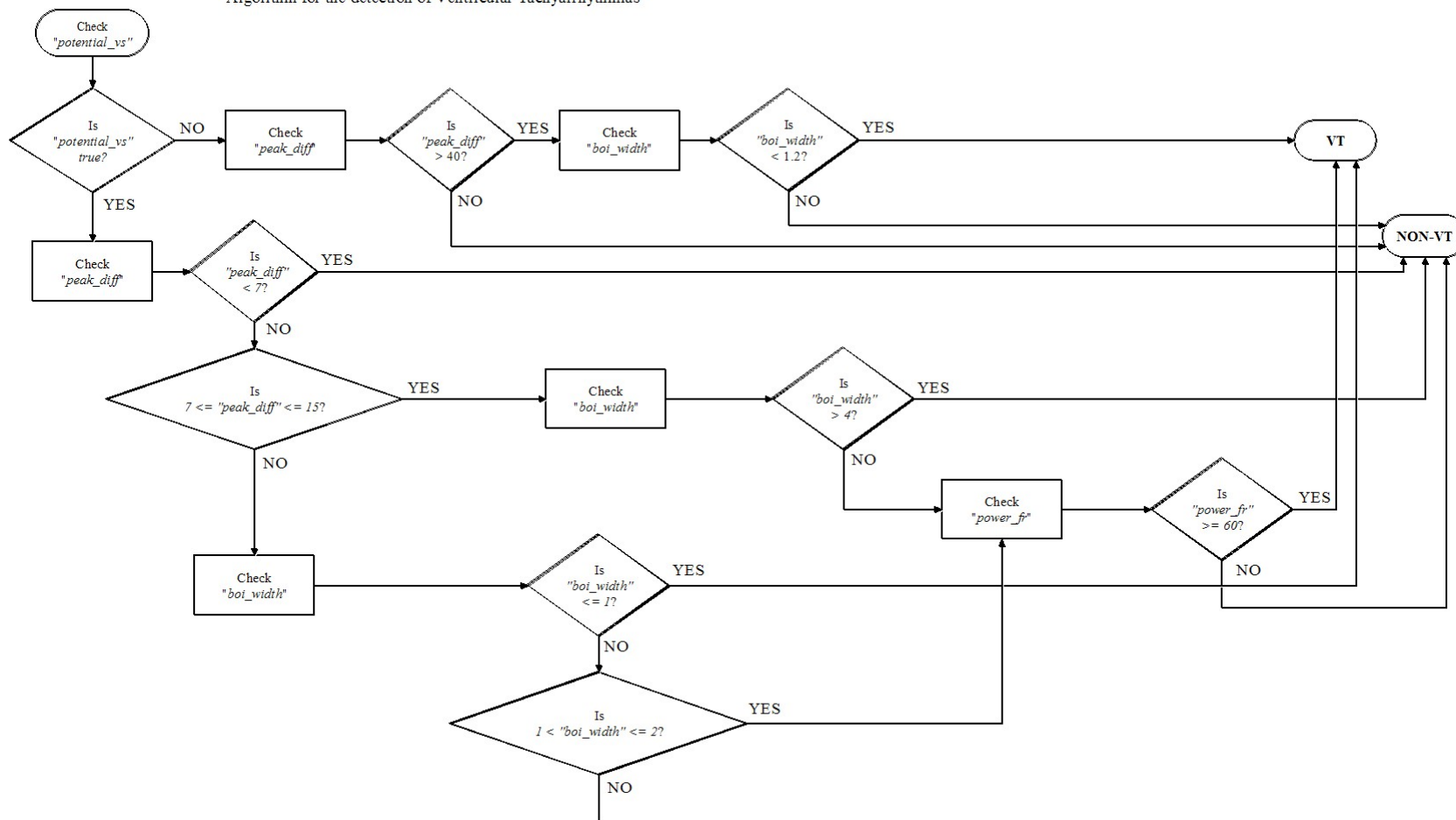


Figure 3.7: Decision flowchart for the detection of ventricular tachyarrhythmias

### 3.2.3.6 AF detection

The main characteristic of an atrial fibrillation ECG is the total disparity of the beat to beat intervals. On the other hand, a rhythmic ECG has all the peak to peak intervals similar to each other. For better comprehension of the specific property of an atrial fibrillation ECG compare figures 3.1 and 1.12. Consequently, it was possible to classify the data series with introduced episodes of atrial fibrillation from the fluctuations in R-R interval values.

However, the computation of these intervals is not always a straightforward procedure. In many cases ordinary peak detection algorithms when applied to the original data set fail due to the complicated nature of the ECG signal. Moreover, depending on the lead used for data acquisition an ECG could comprise more than one close located peaks with similar amplitudes within one heart beat. Not to mention the possible addition of noise. Therefore a peak detection algorithm that is based on a threshold when applied directly to an ECG could easily be confusing.

To overcome this, a peak detection algorithm was applied not directly to the initial ECG time series but rather on the *scale-averaged wavelet power spectrum* of it. The band of scales utilized in the computation of the SAWPS was the corresponding band of frequencies with one Hertz lower bound and upper bound the maximum frequency used in the transform. It is obvious that R-R interval estimation is more convenient when performed on this spectrum rather than on the original data set. Figure 3.8 illustrates the SAWPS over the specified band of the atrial fibrillation ECG signal of figure 1.12.

In the SAWPS the local maxima were first estimated. Thereafter, a threshold rejects those local peaks that are lower than that. The threshold selected in this case consisted of the sum of the mean value and the standard deviation of the *scale-averaged wavelet power*. This action was performed in order to discard some low power peaks that sometimes appear at the adjacency of the true power maxima. It is an effect of the coexistence of two high peaks within the same heart beat. Finally, the peak to peak intervals of the residual local maxima were estimated, while the first and the last of these intervals were rejected for discontinuity reasons at the edges of the data series.

Afterwards, a histogram of these beat to beat intervals was calculated. The bins utilized in the histogram computation had resolution equal to 0.05. The choice of the resolution has concluded from different implementations of various histograms (from rhythmic and atrial fibrillation ECG signals). These implementations have shown that it is a sufficient value. However, smaller values could also be used instead at the expense of a small increment in computational complexity.

From the computed histogram two parameters were estimated in order to characterize the diversity of all intervals. The diversity refers not only to the quantity of the different values of R-R periods but also to the extent of this difference itself. The first variable is called “*max\_elem\_percent*” and it concerns the maximum amplitude of the histogram. More specifically, it expresses the percentage of the maximum number of similar intervals in respect to the number of all the calculated intervals. The second one, the “*disperse\_bins\_percent*”, represents the percentage of those periods which are far from the maximum amplitude of the histogram at distance larger than a selected threshold. This threshold was chosen to be equal to 0.1, which is twice as the precision of the bins used.

Depending on the values of the above parameters it is possible to distinguish between the ECG data series with atrial fibrillation. This classification process was performed along with the premature beat contractions detection (which is described in the following section) in one unified algorithm. The flow chart of this algorithm is shown in figure 3.10. Figure 3.9 illustrates three histograms resulted from the analysis of a NSR, a PC and an AF ECG recording. The dispersion of the R-R intervals is characteristic for each signal category.

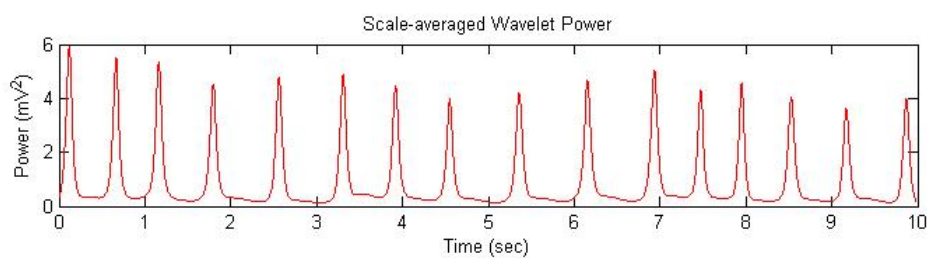


**Figure 3.8:** *The scale-averaged wavelet power over the specified band of the atrial fibrillation ECG signal of figure 1.12*

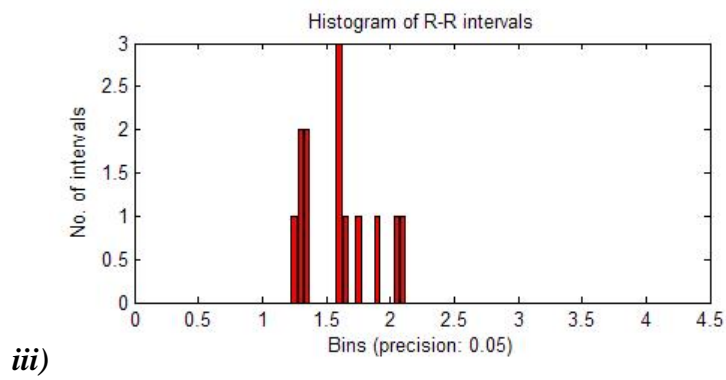
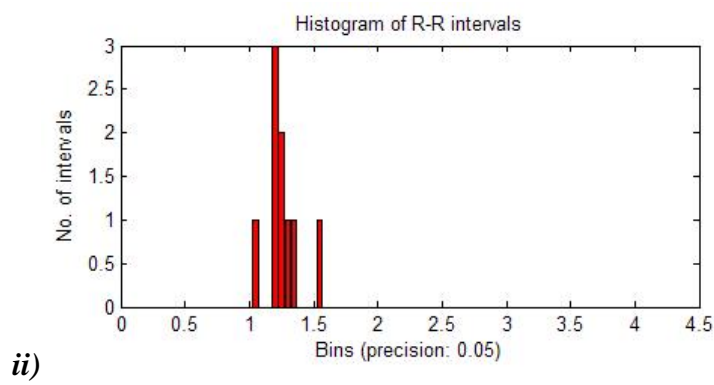
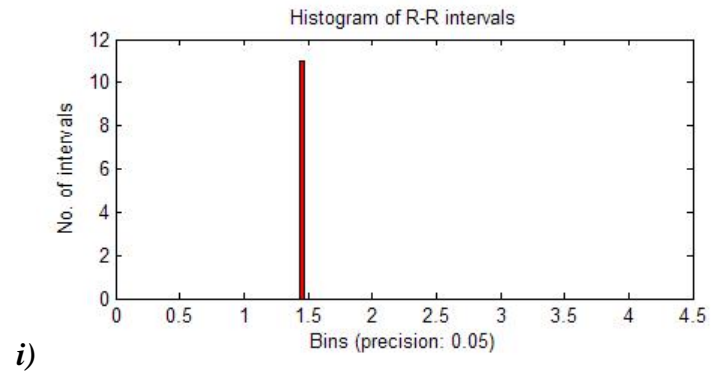


**Figure 3.9:** The distribution of the R-R intervals of *i)* a NSR, *ii)* a PAC and *iii)* an AF signal

### 3.2.3.7 PC detection

The data series with introduced premature contractions (atrial or ventricular) had fewer similar R-R intervals comparable to those in rhythmic ECG signals. At the same time they also had fewer unequal R-R intervals than ECG experienced with atrial fibrillation.

It was therefore obvious that time series with introduced ectopic beats constitute an intermediate situation between the rhythmic and the atrial fibrillation signals with regard to the heart rhythm. Therefore, following the same methodology described in the previous section the classification amongst the rhythmic ECG data series, atrial fibrillation episodes and ECG signals with the presence of premature beats was possible. As mentioned previously one unified algorithm was able to perform the above taxonomy. This procedure is illustrated in a flowchart in figure 3.10.

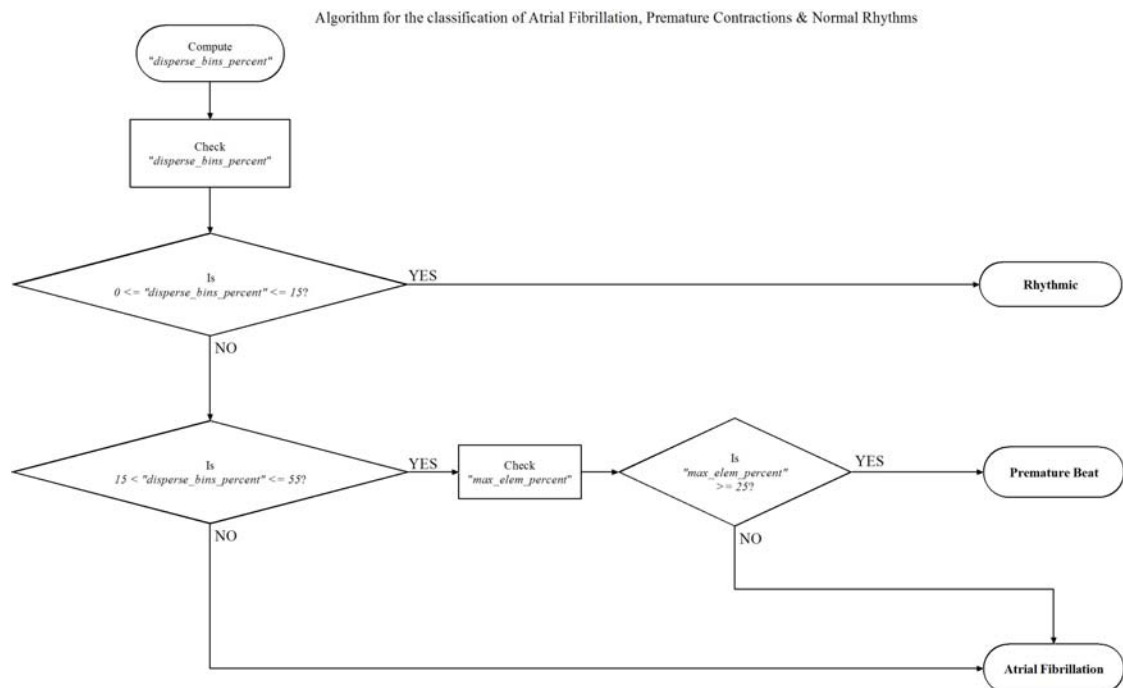


**Figure 3.10:** Decision flowchart for the detection of atrial fibrillation, premature contractions and rhythmic signals

### *3.2.3.8 HR estimation*

As long as the ECG signal is free from ventricular tachyarrhythmia episodes the heart rate parameter in beats per minute (BPM) was calculated. The beats per minute could be estimated by the number of R-R intervals existing through the available length of the ECG recording in cases of unequal beat to beat intervals existence as mentioned in the Medical Background section. This method, of course, could also be applied to rhythmic ECG signals. Consequently, the already calculated peak to peak intervals are counted and then the resultant number was multiplied by six since the duration of each record analyzed in this case was equal to ten seconds. The outcome constituted the requested BPM parameter.

Every ECG time series for which the BPM was calculated could be characterized by normal rate, bradycardia or tachycardia. This characterization was based upon the value of BPM. Therefore, when BPM was within the range [50-100] then the signals have normal heart rate. In cases where the heart rate was lower than 50 beats per minute bradycardia was diagnosed whereas when the heart rate was higher than 100 beats per minute tachycardia was indicated.

### *3.2.3.9 ST, SB and NSR detection*

After the last classification of the ECG signal into the three categories (normal heart rate, bradycardia and tachycardia) according to the heart rate, the assessed heart rhythm parameter could be combined in order to expand the classification process further. Therefore, when the heart rhythm and the heart rate are normal then the normal sinus rhythm describes the ECG data series. Moreover, a combination of a reduced heart rate (<50 BPM) in a rhythmic ECG results in sinus bradycardia. On the other hand, an increased heart rate (>100 BPM) combined with rhythmic time series leads to the characterization of sinus tachycardia.

### *3.2.4 Classification*

This section describes the overall classification process. This was initiated with the calculation of the different frequency bands within the GWS, which helped in the estimation of the VT parameters as outlined in section 3.2.3.4. Then, the classification procedure was mainly separated into two parts. At the first part, the ECG recording was checked for a potential ventricular tachyarrhythmia episode existence. The variables described at section 3.2.3.5 were estimated and the decision flowchart illustrated in figure 3.7 was performed. Therefore, if any ventricular tachyarrhythmia disturbance was traced the analysis stopped.

On the contrary, if no ventricular tachyarrhythmia could be detected by the VT parameters the flow was shifted to the second part and the R-R intervals were estimated. In the case when no peak to peak intervals were able to be computed then the control flow stops as VT is highly suspected. Otherwise the histogram of these peak to peak intervals was calculated. Therefore, the next parameters (AF parameters) - mentioned at section 3.2.3.6 - were calculated. Then, the second decision flowchart shown in figure 3.10 was followed in order to classify the ECG signals into three categories: (i) into those with atrial fibrillation, (ii) those with introduced premature contractions and (iii) those that were rhythmic.

Afterwards, the heart rate was calculated. The value of the beats per minute determined bradycardia, tachycardia or normal heart rate ECG time series. In the special occasion where the analysed data was rhythmic then the characterization of the ECG signal was split into three new categories concerning sinus bradycardia, sinus tachycardia and normal sinus rhythm. All the classification procedure is presented in the following flow diagram as shown in figure 3.11.

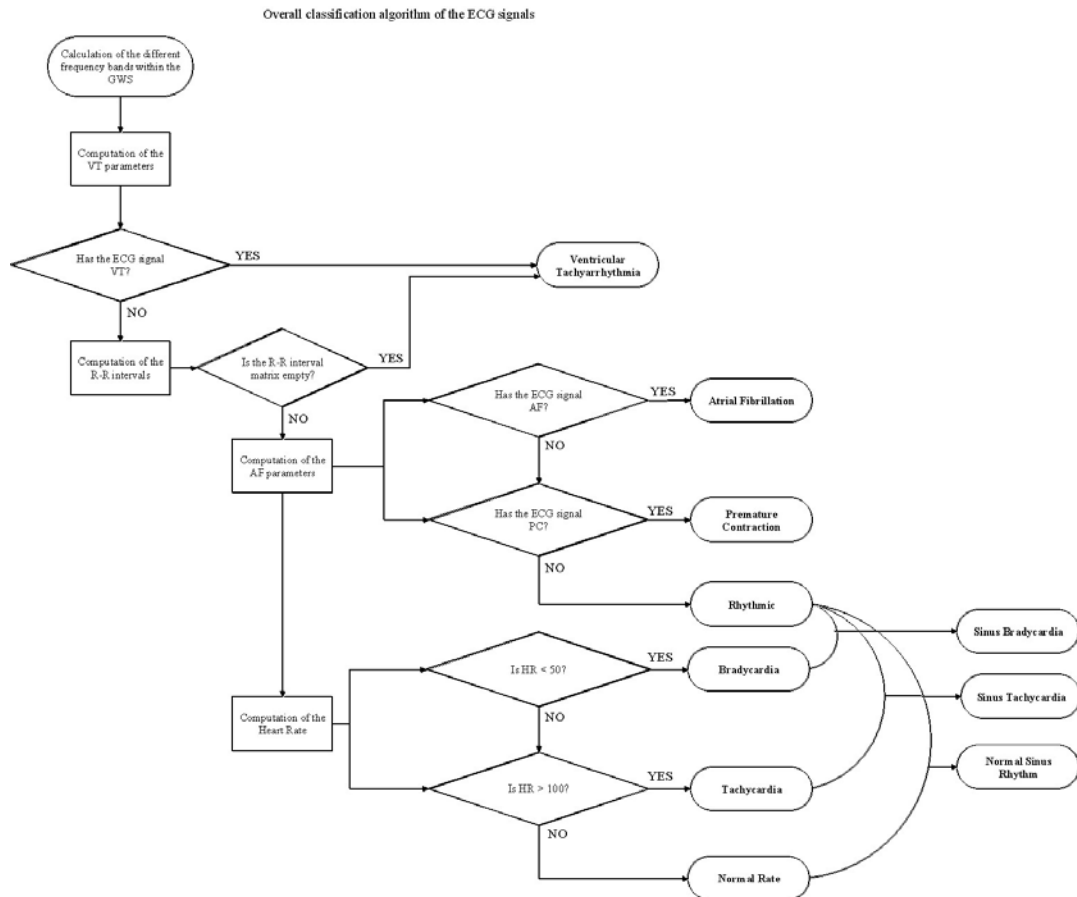


**Figure 3.11:** Overall classification process of the ECG signals

### 3.3 Software presentation

#### 3.3.1 Input variables

The software utilized for the signal analysis was developed in MATLAB. The executable file was named “*ecg\_analysis.m*”. Initially the program asks from the user to load an ECG time series to analyse. This is performed by the dialog window illustrated in figure 3.12. After loading the data the user should determine some parameters for the analysis. The first parameter concerns the location of the ECG data series within the “.dat” file. When more than one ECG recordings from different leads are available in the data file then this variable is used for choosing the preferred signal. For example, this parameter should be set equal to one when the data file

contains only the desirable signal. The second variable is the sampling frequency utilized during the discretization process. The third parameter is the frequency threshold used in the wavelet analysis in order to reject frequencies (scales) in which the influences are not negligible. The last two variables specify the band of interest. Remember that this band determines the region of GWS in which ventricular tachyarrhythmia characteristics are the mostly concentrated. The dialog window in figure 3.13 shows all the input parameters.

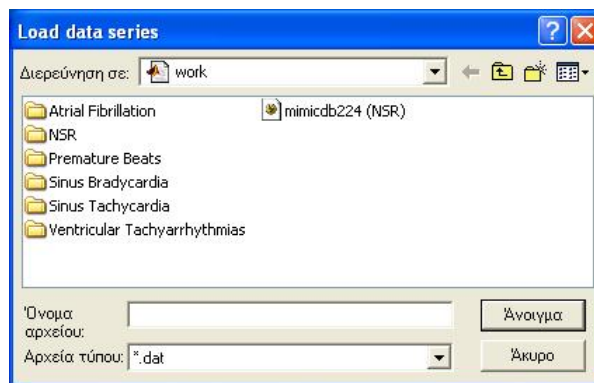


**Figure 3.12:** Dialog window for loading the data series

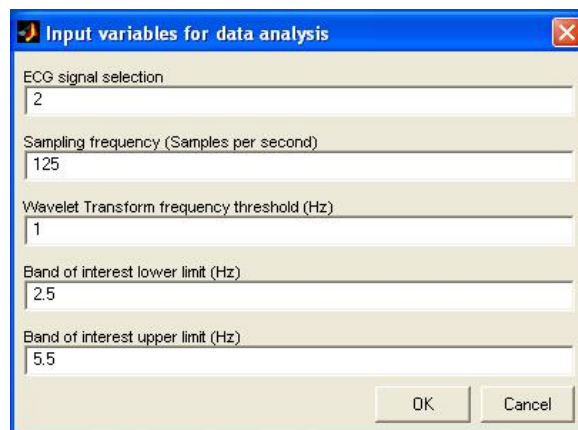


**Figure 3.13:** Dialog window for loading the input variables

### 3.3.2 Program output

Five representative outputs, one of each ECG signal category (NSR, Sinus Tachycardia, Premature Contraction, Atrial Fibrillation and Ventricular Tachyarrhythmia), are illustrated in figures 3.14, 3.15, 3.16, 3.17 and 3.18 respectively.

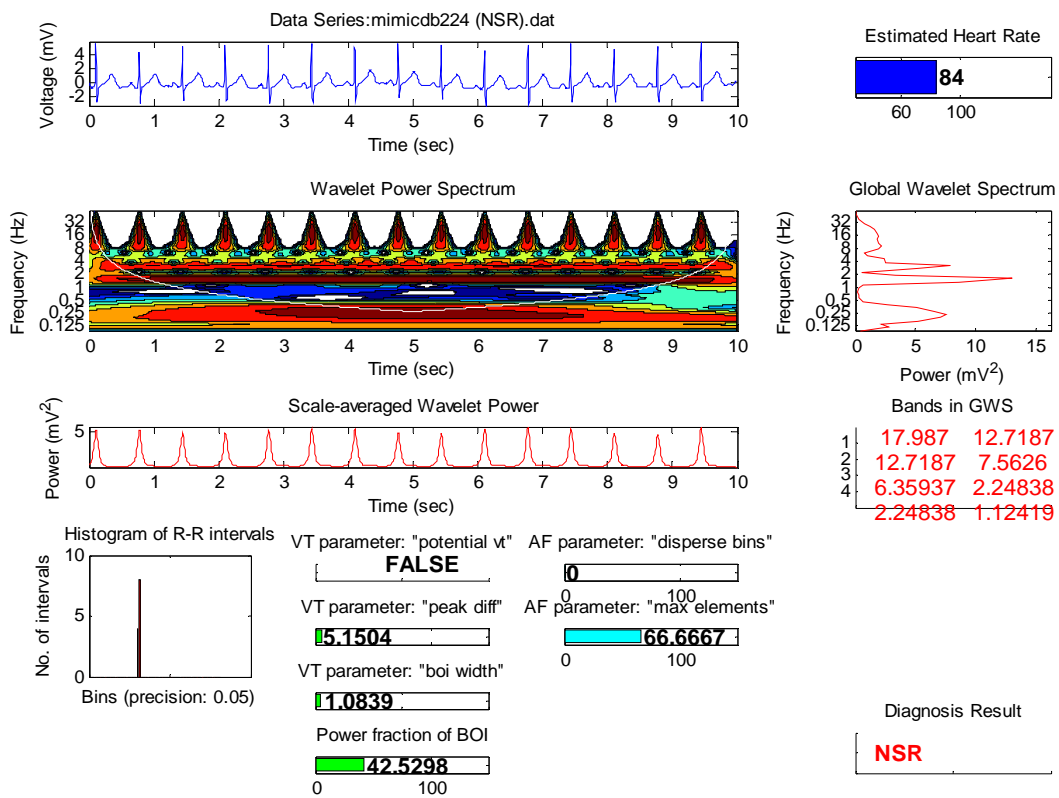


Figure 3.14: Output for a NSR ECG signal

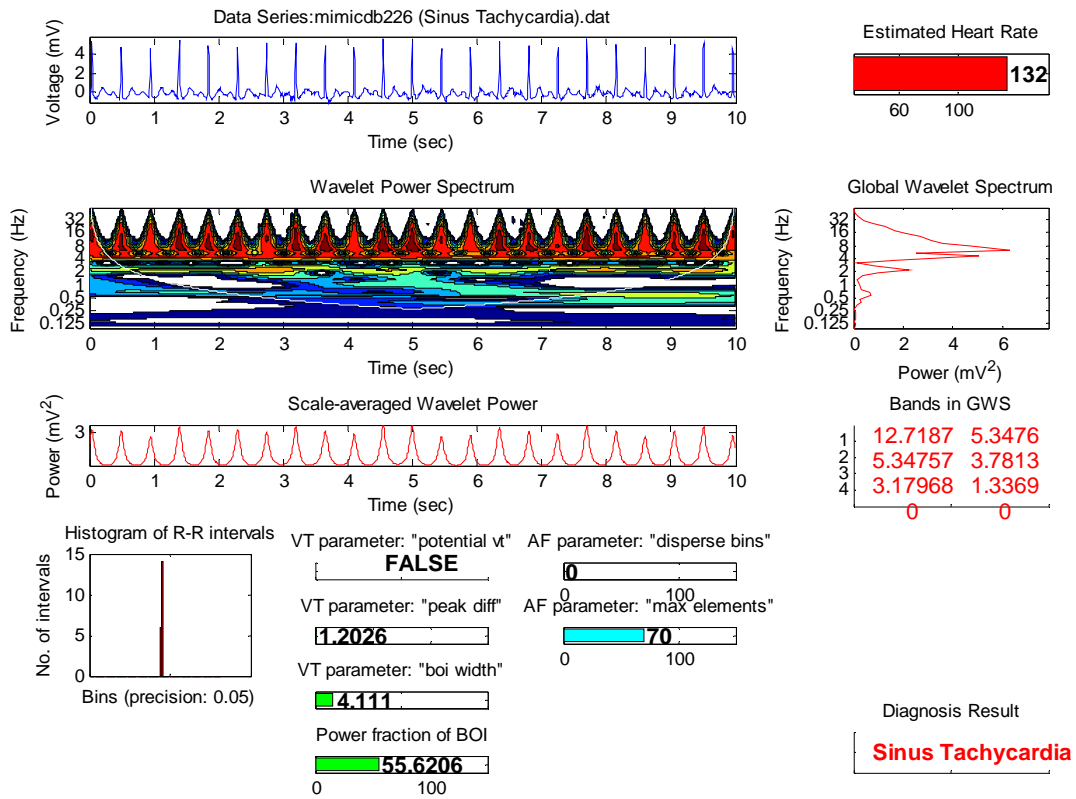


Figure 3.15: Output for an ECG signal during Sinus Tachycardia

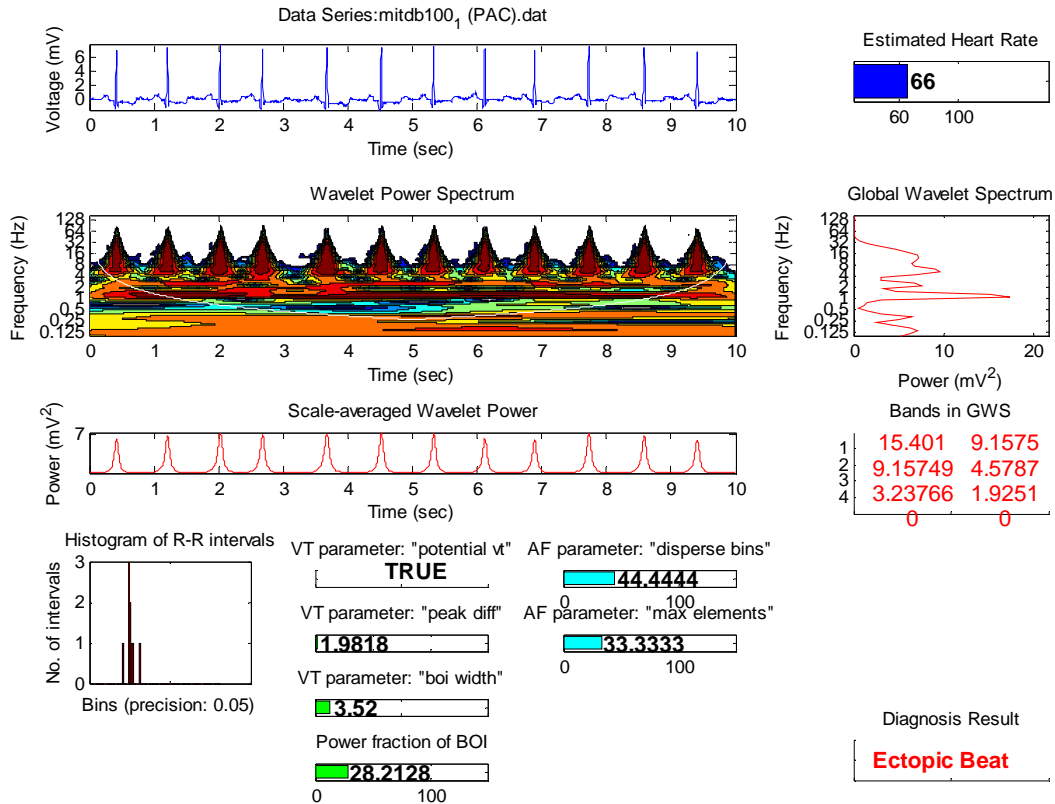


Figure 3.16: Output for an ECG signal with an introduced PAC

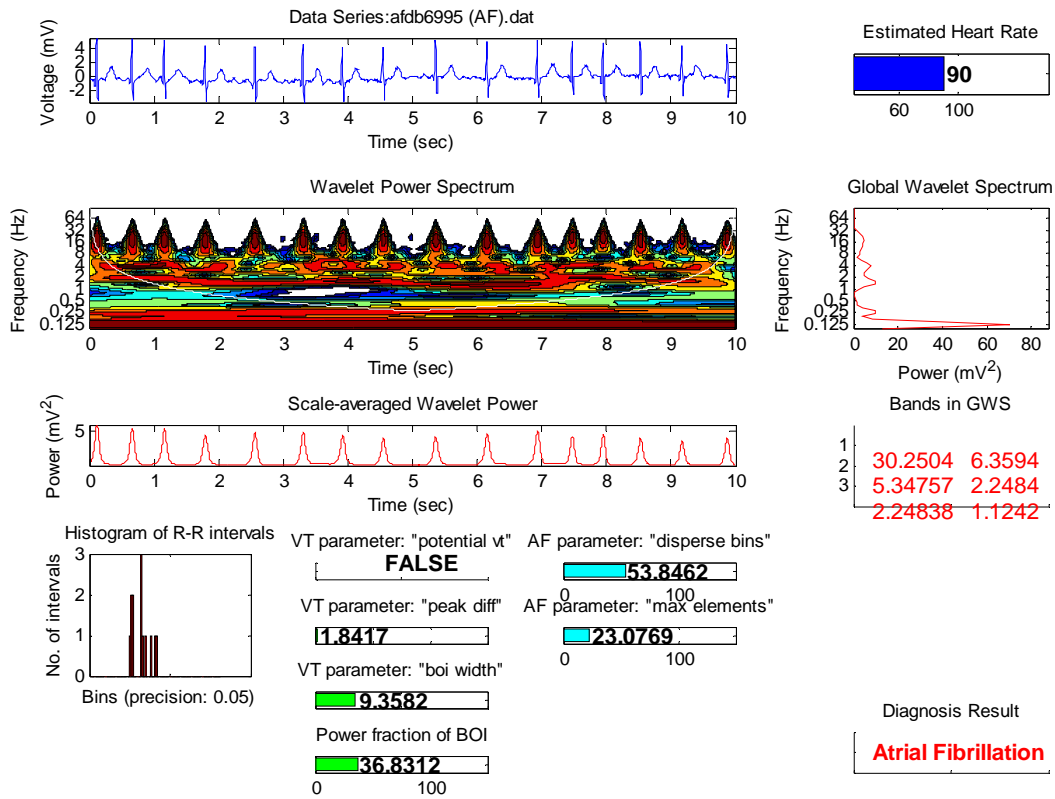


Figure 3.17: Output for an ECG signal during Atrial Fibrillation

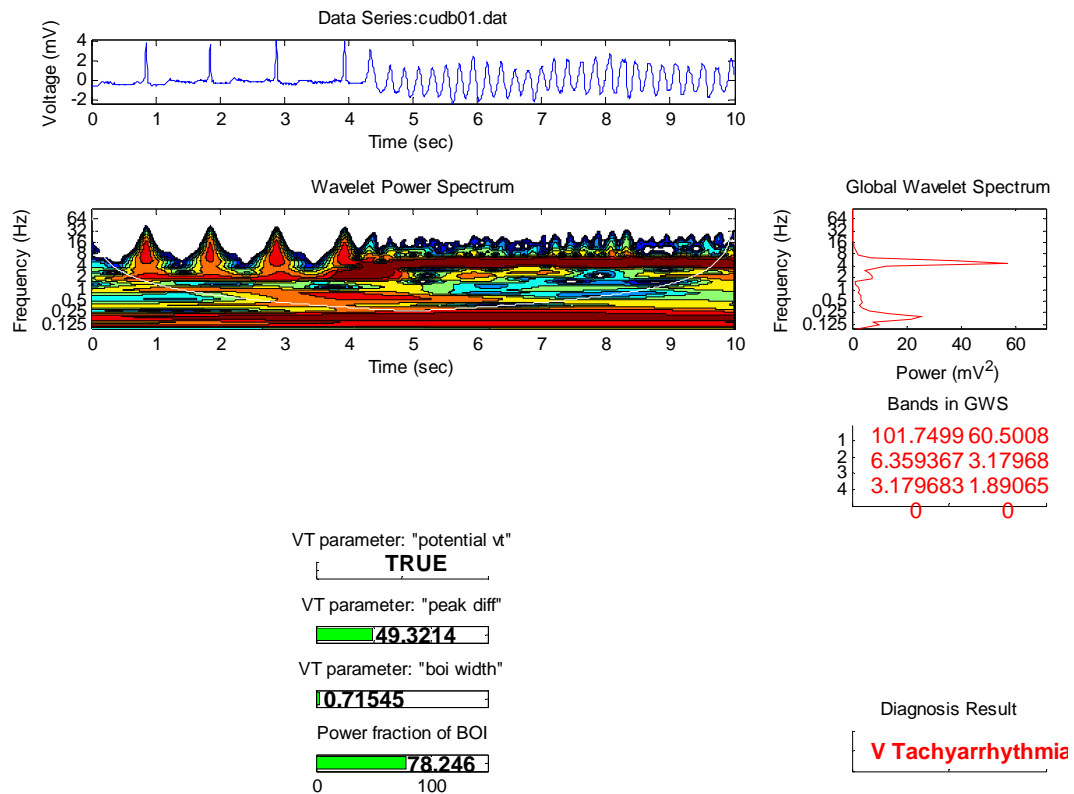


Figure 3.18: Output for an ECG signal during Ventricular Tachyarrhythmia

## 4. RESULTS

### *4.1 Parameters distribution*

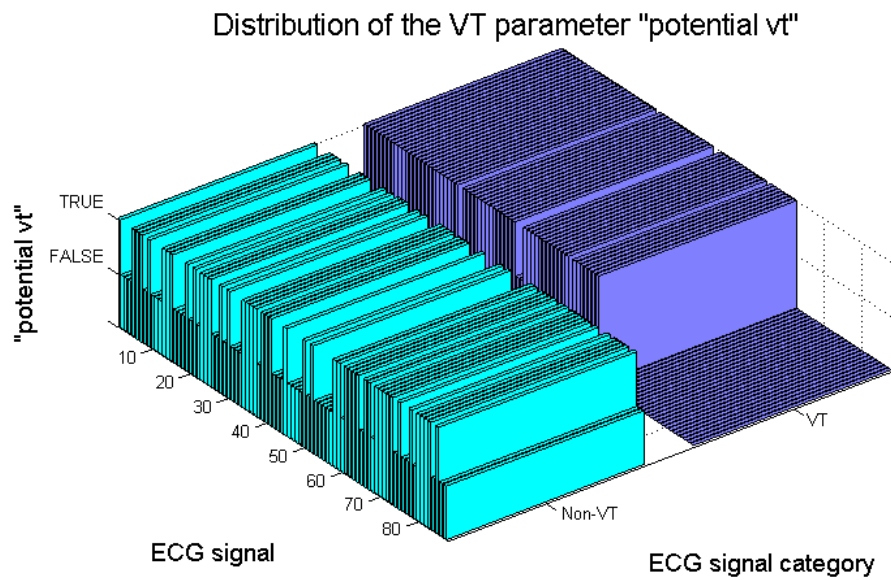
#### *4.1.1 Distribution of the VT parameters*

A total number of 149 ECG recordings of ten seconds duration each were analysed. The different parameters (VT and AF) were estimated in order to find the distribution of them with regard to every ECG signal category. Thus, the first separation of the ECG data series into the two large subclasses of those with or without experienced ventricular tachyarrhythmia episodes was performed by the VT parameters. The fluctuations of the first VT parameter (“*potential\_vt*”) are illustrated in figure 4.1 for all the ECG’s (i) and for the non-VT signals (ii) and the VT signals (iii) separately in histograms. As this figure reveals with the use of this variable a sufficient number of ECG signals without VT episodes was successfully discarded. On the other hand, only a few detections concerning VT signals were missed. Note that values which lie on the x-y plane are not corresponding to ECG signals since the number of the analysed samples of each ECG category is not equal.

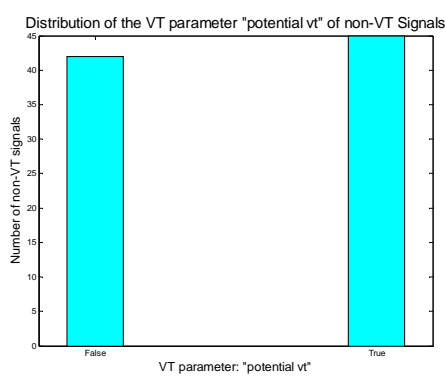
The fluctuations of the next parameter (“*peak\_diff*”) are shown in figure 4.2. It is apparent that the values for the VT case are generally greater comparing to those in the non-VT case. The contrary scene is observed in figure 4.3 where the distribution of the “*boi\_width*” parameter is picturized.

The distribution of the last VT variable examined is illustrated in figure 4.4 from where mainly two observations can be obtained. The first concerns the non-VT signals and is the fact that the “*power\_fr*” fluctuates among intermediate values whereas there are some signals with relatively large power percentage. The second one deals with the VT time series where the majority of the “*power\_fr*” is above 60% while a small percentage is below this value.

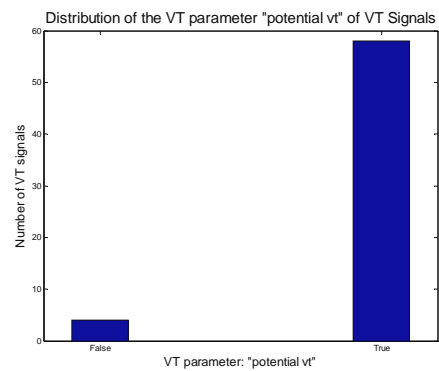
Figure 4.5 shows the feature space for the last three variables (“*peak\_diff*”, “*boi\_width*”, “*power\_fr*”), while table 4.1 summarizes the distribution of each VT parameter based on selected thresholds.



i)



ii)



iii)

**Figure 4.1:** i) Distribution of the “*potential\_vt*”, ii) Histogram of the “*potential\_vt*” of non-VT signals, iii) Histogram of the “*potential\_vt*” of VT signals.

Distribution of the VT parameter "peak diff"

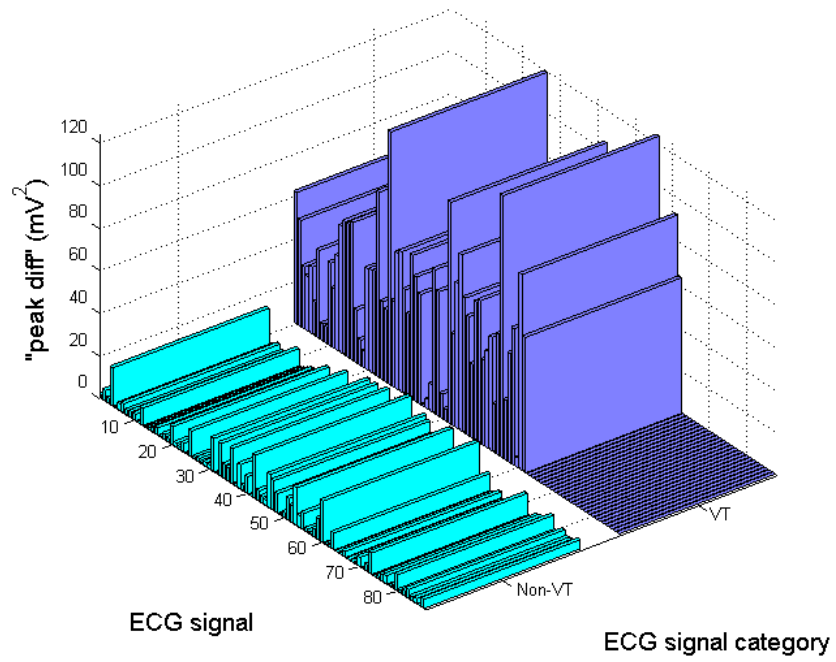


Figure 4.2: Distribution of the "peak\_diff"

Distribution of the VT parameter "boi width"

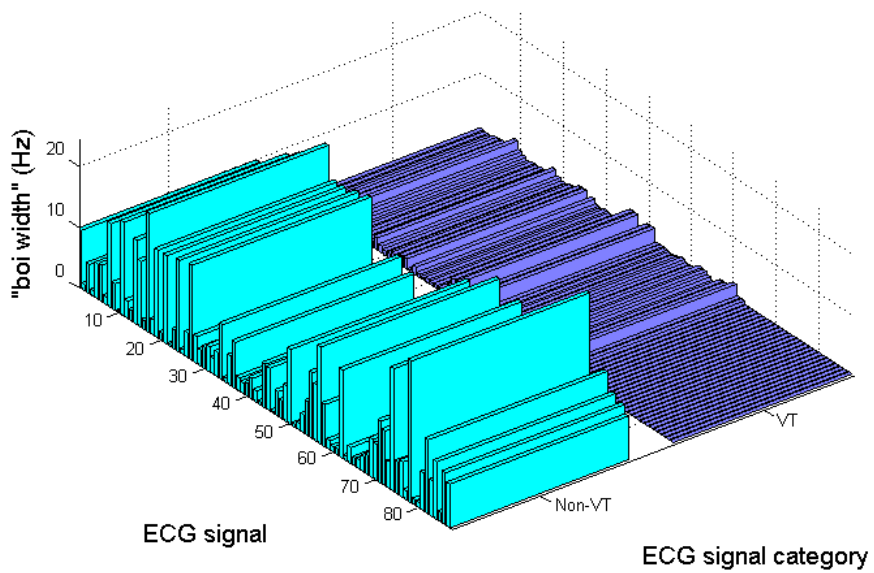
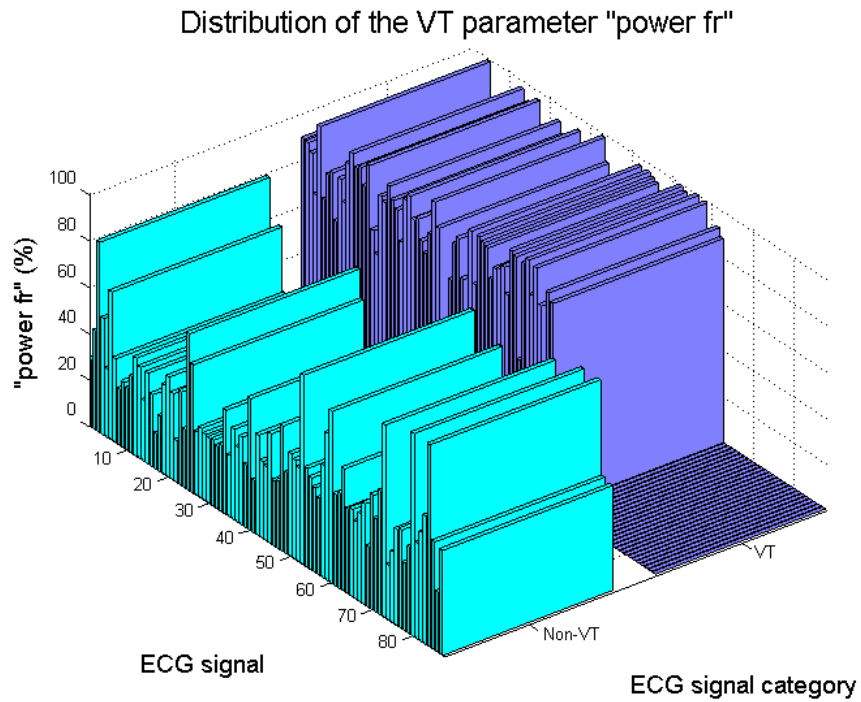
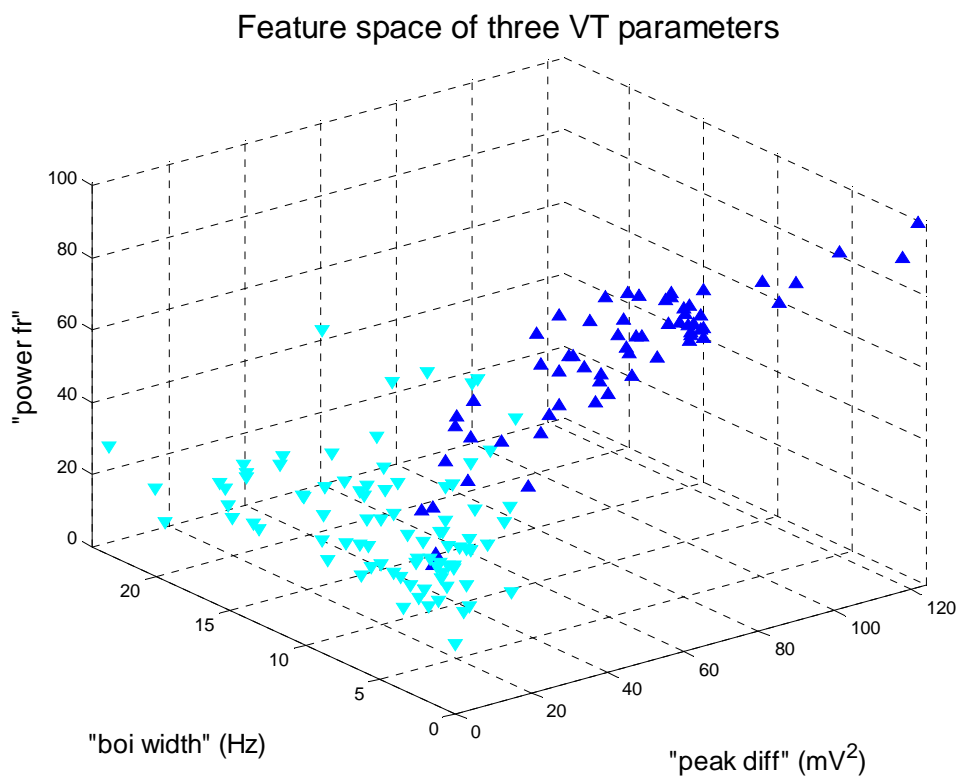


Figure 4.3: Distribution of the "boi\_width"



*Figure 4.4: Distribution of the "power\_fr"*



*Figure 4.5: Feature space of the VT parameters ("peak\_diff", "boi\_width" and "power\_fr"). The blue upward pointing triangles correspond to VT signals, while the cyan downward pointing triangles correspond to non-VT signals.*

VT parameters	“potential_vt” <i>(true or false)</i>		“peak_diff” <i>(thres = 7)</i>		“boi_width” <i>(thres = 1.2)</i>		“power_fr” <i>(thres = 60)</i>	
	False (%)	True (%)	< <i>thres</i> (%)	> <i>thres</i> (%)	< <i>thres</i> (%)	> <i>thres</i> (%)	< <i>thres</i> (%)	> <i>thres</i> (%)
<i>Normal Sinus Rhythm</i>	<b>50</b>	<b>50</b>	<b>87.5</b>	<b>12.5</b>	<b>16.7</b>	<b>83.3</b>	<b>83.3</b>	<b>16.7</b>
<i>Sinus Tachycardia</i>	<b>60</b>	<b>40</b>	<b>80</b>	<b>20</b>	<b>20</b>	<b>80</b>	<b>80</b>	<b>20</b>
<i>Premature Contractions</i>	<b>50</b>	<b>50</b>	<b>55.6</b>	<b>44.4</b>	<b>16.7</b>	<b>83.3</b>	<b>100</b>	<b>0</b>
<i>Atrial Fibrillation</i>	<b>45</b>	<b>55</b>	<b>75</b>	<b>25</b>	<b>20</b>	<b>80</b>	<b>85</b>	<b>15</b>
<i>Ventricular Tachyarrhythmias</i>	<b>6.5</b>	<b>93.6</b>	<b>6.5</b>	<b>93.6</b>	<b>74.2</b>	<b>25.8</b>	<b>8.1</b>	<b>91.9</b>

**Table 4.1:** Distribution of each VT parameter based on selected thresholds

### 4.1.2 Distribution of the AF parameters

The second classification step was performed by the estimation of the AF variables. The distributions of these two parameters (“*disperse\_bins\_percent*” and “*max\_elem\_percent*”) are illustrated in figures 4.6 and 4.7, respectively. From the fluctuations of the “*disperse\_bins\_percent*” one can derive the next remarks:

-  **NSR:** Generally they have very small values of “*disperse\_bins\_percent*” whereas in some few cases these values could reach higher.
-  **Sinus tachycardia:** A similar distribution as in the NSR category is observed here apart from the higher peaks.
-  **Premature contractions:** In the ectopic beats case, the major fluctuations of the parameter “*disperse\_bins\_percent*” construct a band with values greater than in the two last cases.
-  **Atrial fibrillation:** The distribution of the “*disperse\_bins\_percent*” for the atrial fibrillation case has an expected topology. Furthermore, although the fluctuations in this signal category are somewhat similar to those in the premature contraction case they appear slightly concentrated in a higher band. This is the basic reason why the next parameter was introduced: To improve the discrimination process between the ECG signals with introduced ectopic beats and those with atrial fibrillation episodes.

The distribution of the second parameter “*max\_elem\_percent*” through the different ECG signals presents the complete opposite topology from the one shown in the first AF variable. That is high values for the NSR and the sinus tachycardia cases and lowers for the ectopic beat and the atrial fibrillation signals.

Figure 4.8 illustrates the feature space of (i) the “*disperse\_bins\_percent*” and (ii) the “*max\_elem\_percent*”, while table 4.2 summarizes the distribution of each AF parameter based on selected thresholds.

Distribution of the AF parameter "disperse bins percent"

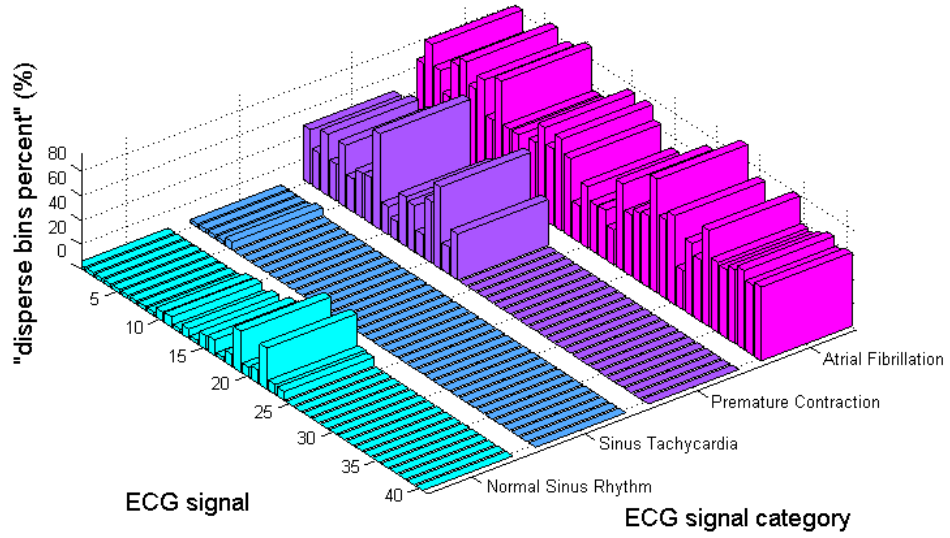


Figure 4.6: Distribution of the "disperse\_bins\_percent"

Distribution of the AF parameter "max elem percent"

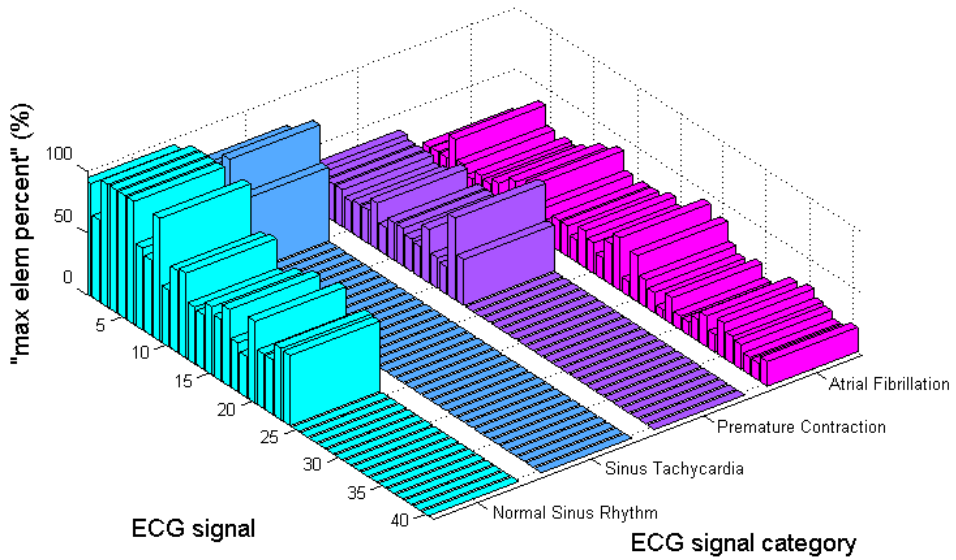
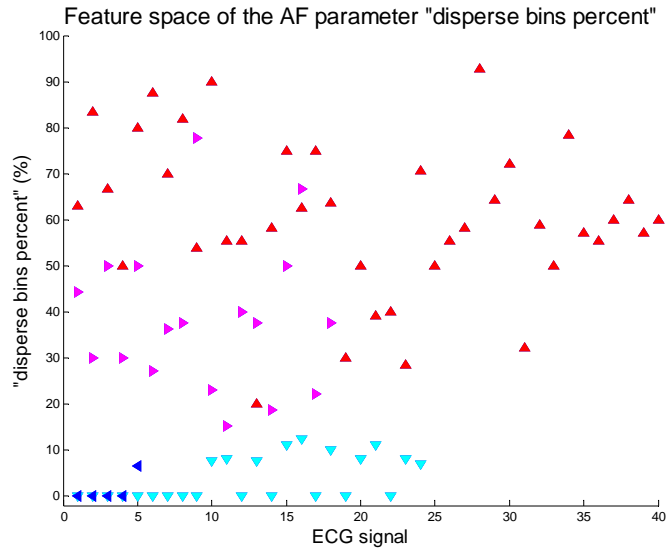
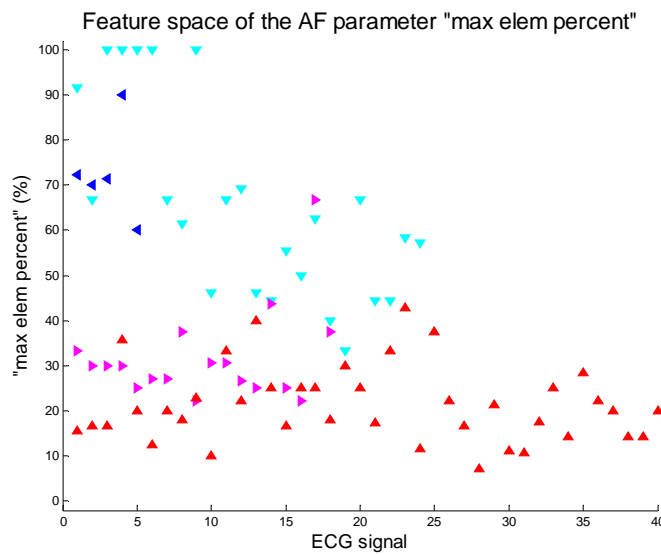


Figure 4.7: Distribution of the "max\_elem\_percent"



i)



ii)

**Figure 4.8:** (i) Feature space of the AF parameter “disperse\_bins\_percent”. (ii) Feature space of the AF parameter “max\_elem\_percent”. The cyan downward pointing triangles correspond to NSR signals, the blue left pointing triangle correspond to Sinus Tachycardia signals, the magenta right pointing triangles correspond to Ectopic Beats signals and the red upward pointing triangles correspond to Atrial Fibrillation signals.

<b>VT parameters</b>	<b>“disperse_bins_percent”</b>		<b>“max_elem_percent”</b>	
<b>ECG category</b>	<b>&lt; thres (%)</b>	<b>&gt; thres (%)</b>	<b>&lt; thres (%)</b>	<b>&gt; thres (%)</b>
	<i>(thres1 = 15)</i>		<i>(thres = 25)</i>	
<i>Normal Sinus Rhythm</i>	<b>91.7</b>	<b>8.3</b>	<b>0</b>	<b>100</b>
<i>Sinus Tachycardia</i>	<b>100</b>	<b>0</b>	<b>0</b>	<b>100</b>
	<i>(thres2 = 55)</i>		<i>(thres = 25)</i>	
<i>Premature Contractions</i>	<b>88.9</b>	<b>11.1</b>	<b>11.1</b>	<b>88.9</b>
<i>Atrial Fibrillation</i>	<b>25</b>	<b>75</b>	<b>77.5</b>	<b>22.5</b>

**Table 4.2:** Distribution of each AF parameter based on selected thresholds

## 4.2 ECG classification results

The extracted classification results for each ECG signal category are the following.

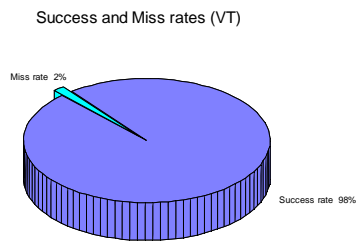
-  **Ventricular tachyarrhythmia:** A total number of 62 ECG signals with ventricular tachyarrhythmia episodes were used in the current analysis. The discrimination procedure followed was unable to characterize only one VT signal, while the rest of them were classified correctly.
  
-  **Atrial fibrillation:** A total number of 40 ECG data series experienced with atrial fibrillation episodes were analysed here. Six of them were classified incorrectly as premature contraction beats while one of them was wrongly characterized as ventricular tachyarrhythmia. The latter signal had similar characteristics as the VT signal in the GWS. The other six that referred as PC were in a way justifiably featured like this because their features were in the borderline between the AF and the PC category.
  
-  **Premature contraction:** From the ectopic beat category there were only 18 ECG signals available. These recordings contained one or two premature contractions either atrial or ventricular. From them only two were featured as AF data series. The reason is the same as with the AF case discussed in the preceding section. Note that a ten second signal with two introduced ectopic beats can easily be perceived as an AF signal, since one ectopic beat corresponds to two different R-R intervals.
  
-  **Sinus tachycardia:** In this signal category only 5 ECG record were available. All of them were distinguished from the others except for one. This record has similar behaviour with a VT signal that's why it was characterized proportionally.
  
-  **NSR:** The number of NSR ECG recordings that were analysed in this project was equal to 24. Only the two of them were incorrectly classified as time series with introduced premature contractions. However, this is substantially justifiable by the fact that these exceptions present a slight degree of arrhythmia (Sinus arrhythmia).

Therefore, the classification algorithm utilized performs the discrimination of the NSR signals in a very sufficient way.

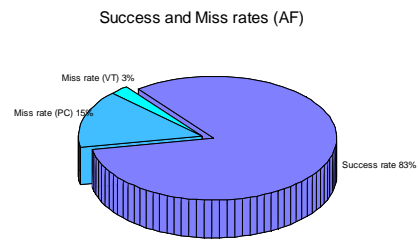
### *4.3 ECG classification rates*

Figure 4.9 illustrates graphically the success and the miss classification rates of each ECG signal category, while table 4.3 concentrates on the success rate (precision), the miss rate and the misclassification rate (sensitivity) of all the ECG signals analysed in this project. From table 4.3 it can be observed that the success rates are relatively large, while the misclassification rates are very small, almost negligible in the majority of the ECG signal categories.

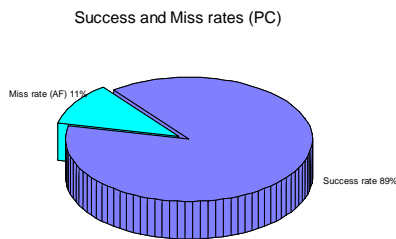
Figure 4.10 shows the success and the miss classification rates of the total number of the classified ECG recordings. The overall success rate concerns the total efficiency (precision) of the discrimination algorithm utilized in this project. As it can be derived from the results, the percentage of the overall miss rate is relatively small. However, this rate is possible to be improved by rejecting some “inappropriate” signals like the ones used in the NSR category (with sinus arrhythmia). However, if a sufficient number of the ECG recordings presenting with this type of arrhythmia was available and with suitable modifications in the classification algorithm it would be an easy step to distinguish between these signals and include them into a new ECG category. Moreover, the overall miss rate could potentially be reduced by introducing new parameters used for the distinction of the premature contractions from the atrial fibrillation recordings.



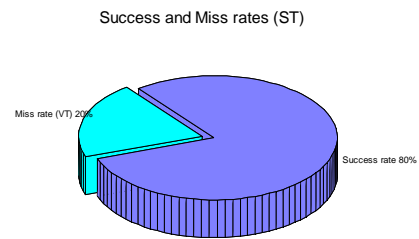
*i) VT classification rates*



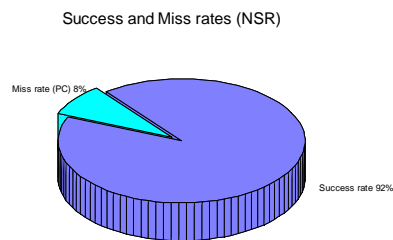
*ii) AF classification rates*



*iii) PC classification rates*



*iv) ST classification rates*



*v) NSR classification rates*

**Figure 4.9:** Success and miss classification rates of (i) VT, (ii) AF, (iii) PC, (iv) ST and (v) NSR ECG recordings

<b>ECG category</b>	<b>Success Rate (%)</b>	<b>Miss Rate (%)</b>	<b>Misclassification Rate (%)</b>
<i>Normal Sinus Rhythm</i>	<b>91.7</b>	<b>8.3</b>	<b>0</b>
<i>Sinus Tachycardia</i>	<b>80</b>	<b>20</b>	<b>0</b>
<i>Premature Contractions</i>	<b>88.9</b>	<b>11.1</b>	<b>6.9</b>
<i>Atrial Fibrillation</i>	<b>82.5</b>	<b>17.5</b>	<b>1.8</b>
<i>Ventricular Tachyarrhythmias</i>	<b>98.4</b>	<b>1.6</b>	<b>2.3</b>

**Table 4.3:** Success rate, miss rate and misclassification rate of each ECG signal category

### Overall Success and Miss rates

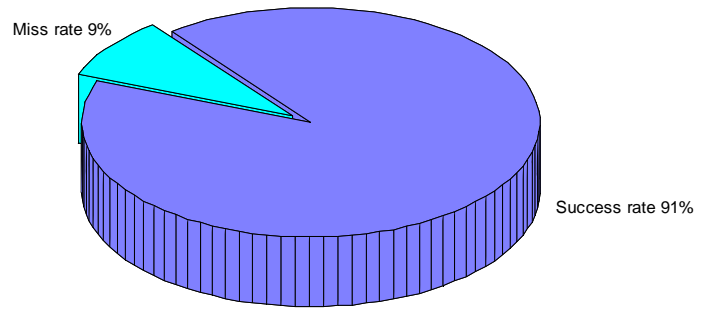


*Figure 4.10: Overall classification rates*

## 5. CONCLUSIONS AND FURTHER WORK

This project examined some of the most common types of arrhythmias encountered in the majority of the human population starting from the less serious such as sinus tachycardia, sinus bradycardia - even if no ECG recordings were available for this type of arrhythmia, the classification algorithm is able to distinguish them - and premature contractions to the more severe atrial fibrillation and the malignant ventricular tachyarrhythmias. A uniform classification algorithm was implemented in order to detect any type of the above set of arrhythmias.

The proposed classification method was able to detect the non-rhythmic from the rhythmic ECG signals in all cases. The discrimination between the non-rhythmic ECG recordings was generally very efficient especially in the critical case of VT where immediate intervention is required. The algorithm was also efficient in the classification of the PC and the AF ECG data series, although in some cases was misleading. This misleading is totally justified by the fact that the classification procedure for these signals was based on R-R interval estimation and these misclassified PC and AF ECG signals had similar distributions in their R-R interval values. The classification process for the ST ECG signals also performed well, whereas no sufficient number of ECG recordings of this type of arrhythmia was available and thus no definite conclusions could be extracted.

Further investigations could be focused towards reducing the number of false diagnoses. This objective requires the correct discrimination and characterization of the specific features of each ECG signal category. Therefore, as mentioned above, new parameters could be introduced for distinguishing the PC from the AF ECG recordings. One further approach could also be the combination of different parameters derived from the GWS and the computed SAWPS simultaneously, based on the special VT characteristic and utilized for the improvement of the classification method. Moreover the presented method could be extended in order to include other ECG cases as well.

The method proposed in this case is based on simple classification techniques derived from the wavelet transform analysis of the ECG. The most important is that it combines the detection of characteristics appearing on the time (distribution of R-R intervals) and frequency domain (high power peak in GWS). Consequently, the implemented algorithm can be utilized for the characterization of NSR, ST, SB, AC and AF together with different VT ECG recordings. This is realized by taking advantage of the benefits of the *continuous wavelet transform* such as the good time and frequency localization plus the endogenous redundancy, which reinforces the traits and makes all information more visible.

## 6. REFERENCES

- [1] C. J. Wiggers, “The Heart”, *Scientific American*, 1957.
- [2] R. G. Mark, “Biological measurements: Electrical characteristics of the heart”, *Systems & Control Encyclopedia: Theory, Technology, Applications*, Pergamon Press, New York.
- [3] G. Papazaxos, “The electrocardiogram in clinical practice”, *Litsas Medical Publications*, 1982.
- [4] The American Heart Association, on-line: <http://www.americanheart.org>, last accessed on 16.05.03.
- [5] Greek National Institute of Cardiology, “The Heart”, 1996.
- [6] Goldberger AL, Amaral LAN, Glass L, Hausdorff JM, Ivanov PCh, Mark RG, Mietus JE, Moody GB, Peng CK and Stanley HE, “PhysioBank, PhysioToolkit, and PhysioNet: Components of a New Research Resource for Complex Physiologic Signals”, *Circulation* 101(23): e215-e220, 2000 (June 13).  
on-line: <http://circ.ahajournals.org/cgi/content/full/101/23/e215>
- [7] A. V. Oppenheim and R. W. Schaffer, “Discrete-Time Signal Processing”, *Prentice-Hall*, 1999.
- [8] O. Rioul and M. Vetterli, “Wavelets and signal processing”, *IEEE Signal Processing Magazine*, vol. 8, no. 4, pp. 14-38, 1991.
- [9] A. Papoulis, “The Fourier Integral and its Applications”, *McGraw-Hill*, 1987.
- [10] A. Graps, “An Introduction to Wavelets”, *IEEE Computational Science and Engineering*, vol. 2, num. 2, 1995.

- [11] R. K. Young, "Wavelet theory and its applications", *Kluwer Academic Publishers*, 1993.
- [12] C. Torrence and G. Compo, "A practical guide to wavelet analysis", *Bulletin of the American Meteorological Society*, vol. 69, no. 1, pp. 61-78, 1998.  
on-line: <http://paos.colorado.edu/research/wavelets/>
- [13] M. Vetterli and J. Kovacevic, "Wavelets and subband coding", *Prentice-Hall*, 1995.
- [14] S. D. Meyers, B. G. Kelly, and J. J. O'Brien, "An introduction to wavelet analysis in oceanography and meteorology: With application to the dispersion of Yanai waves", *Monthly Weather Review*, vol. 121, no. 10, pp. 2858-2866, 1993.
- [15] I. Daubechies, "Orthonormal Bases of Compactly Supported Wavelets", *Communications on Pure and Applied Mathematics*, vol. 41, pp. 909-996, 1988.
- [16] M. Bahoura, M. Hassani and M. Hubin, "DSP implementation of wavelet transform for real time ECG wave forms detection and heart rate analysis", *Computer Methods and Programs in Biomedicine*, vol. 52, pp. 35-44, 1997.
- [17] A. Englund, K. Hnatkova, P. Kulakowski, P. M. Elliot, W. J. McKenna and M. Malik, "Wavelet decomposition analysis of the signal averaged electrocardiogram used for risk stratification of patients with hypertrophic cardiomyopathy", *European Heart Journal*, vol. 19, pp. 1383-1390, 1998.
- [18] N. Sivannarayana and D.C. Reddy, "Biorthogonal wavelet transforms for ECG parameters estimation", *Medical Engineering and Physics*, vol. 21, pp. 167-174, 1999.

- [19] J. N. Watson, P. S. Addison, G. R. Clegg, M. Holzer, F. Sterz and C. E. Robertson, "A novel wavelet transform based analysis reveals hidden structure in ventricular fibrillation", *Resuscitation*, vol.43, pp. 121-127, 2000.
- [20] Z. Dokur and T. Olmez, "ECG beat classification by a novel hybrid neural network", *Computer Methods and Programs in Biomedicine*, vol. 66, pp. 167-181, 2001.
- [21] J. K. Mell, D. A. Jordan, Y. Xiao, Y. Zheng, J. G. Akar and D. E. Haines, "Wavelet analysis of atrial fibrillation electrograms", *Proceedings of 2003 IEEE International Conference on Acoustics, Speech and Signal Processing (ICASSP-2003)*, Vol. II, pp. 357-360, Hong Kong, April 6-10, 2003.

## 7. APPENDIX

### 7.1 Definitions

#### *The e-folding time*

The e-folding time is defined as the time required for the amplitude of an oscillation to increase or decrease by a factor of e.

#### *Time resolution*

The time resolution of a transform operation is defined as the ability to resolve fine features in the time domain.

#### *Frequency resolution*

The frequency resolution of a transform operation is defined as the ability to resolve fine features in the frequency domain.

### 7.2 Relevant studies

Some other relevant to this project work that has been done in the past few years is listed and briefly described below.

#### *1) DSP implementation of wavelet transform for real time ECG wave forms detection and heart rate analysis*

This first study was published by M. Bahoura, M. Hassani and M. Hubin back in 1997. In this study the DWT is utilized. More specifically, this algorithm combined the wavelet coefficients in order to distinguish QRS complexes, P and T waves from noise, baseline drift or artifacts as each ECG characteristic was excited better at different scales. It was implemented in a DSP (SPROC-1400) for real time detection. For the MIT-BIH Arrhythmia Database, this algorithm was able to detect 99.7% of the QRS complexes [16].

## *2) Wavelet decomposition analysis of the signal averaged electrocardiogram used for risk stratification of patients with hypertrophic cardiomyopathy*

A. Englund et al studied the predictive value of wavelet decomposition in order to identify patients with hypertrophic cardiomyopathy (published in 1998). The proposed method, based on the CWT, was applied in the signal averaged ECG. Several parameters were derived from the wavelet decomposition analysis. The research concluded that the wavelet analysis of predicting sudden death or ventricular fibrillation was limited in patients with hypertrophic cardiomyopathy. However, it could identify patients at risk of dying non suddenly and with non sustained ventricular tachycardia [17].

## *3) Biorthogonal wavelet transforms for ECG parameters estimation*

This second study was conducted by N. Sivannarayana and D.C. Reddy (published in 1999). Biorthogonal wavelets were used in this study and characterization of the parameters of various morphologies of ECG signals as normal or otherwise were performed. The proposed method applied in single normalized ECG beats. Various morphologies were excited better at different scales and amplitudes, durations and various segments and widths could be determined more accurately. The study concluded that even when the signal-to-noise ratios were poor, the proposed method could estimate accurately the said parameters [18].

## *4) A novel wavelet transform based analysis reveals hidden structure in ventricular fibrillation*

Another study performed by James N. Watson et al. and published in 2000 introduced a novel method of examining the surface ECG signal using the CWT. According to this analysis, at higher frequencies the P, QRS and T components were individually resolved according to their frequency makeup and temporal location. The study demonstrated the utility of the wavelet transform as a new method of ECG signal analysis during VF [19].

### *5) ECG beat classification by a novel hybrid neural network*

In this study, performed by Zumray Dokur and Tamer Olmez and published in 2001, a new hybrid neural network structure for ECG beats classification was presented. The method was followed in three stages: ECG normalization, feature extraction process and classification based on an artificial neural network. ECG features were computed using specific DFT and DWT coefficients determined by dynamic programming according to their distribution values. Ten different types of ECG beats were obtained from the MIT-BIH Arrhythmia Database. These beats were classified with a success rate of 96% by using the hybrid structure [20].

### *6) Wavelet analysis of atrial fibrillation electrograms*

This final study was performed by John K. Mell et al and was published in the year 2003. In this study, an algorithm was developed for measuring beat spacing intervals in AF basket catheter electrograms. The algorithm utilizes partial reconstruction of the *continuous wavelet transforms* to extract the amplitude envelope corresponding to beat bodies to give a new signal where beats can be readily identified and the time interval between beats can be accurately quantified. The results presented on chronic AF electrograms suggest that the wavelet-based methods developed in this paper may be useful for identifying spatially localized sources of AF from basket catheter electrograms [21].

From the above studies it can be seen that a lot of attention has been given in the past to the analysis of ECG signals and how these can be utilized to treat cardiac diseases, which makes our study worthwhile.